Nucleic Acids Research, 2025, **53**, gkae1299
https://doi.org/10.1093/nar/gkae1299
Advance access publication date: 7 January 2025
Gene regulation, Chromatin and Epigenetics

Molecular mechanisms underlying allosteric behavior of *Escherichia coli* DgoR, a GntR/FadR family transcriptional regulator

Swati Singh[1], Garima Arya[1], Rajesh Mishra[1], Shivam Singla[1], Akhil Pratap[2], Krishna Upadhayay[3,4], Monika Sharma[2,*] and Rachna Chaba[1,*]

[1]Department of Biological Sciences, Indian Institute of Science Education and Research (IISER) Mohali, Sector 81, Knowledge City, SAS Nagar, Mohali 140306, Punjab, India
[2]Biological Systems Engineering, Plaksha University, Sector 101 alpha, IT City, SAS Nagar, Mohali 140306, Punjab, India
[3]Council of Scientific and Industrial Research—Institute of Microbial Technology, Sector 39A, Chandigarh 160036, India
[4]Academy of Scientific and Innovative Research (AcSIR), Sector 19, Kamla Nehru Nagar, Ghaziabad 201002, Uttar Pradesh, India

[*]To whom correspondence should be addressed. Tel: +91 8146084997; Fax: +91 1722240266; Email: rachnachaba@iisermohali.ac.in
Correspondence may also be addressed to Monika Sharma. Tel: +91 7087543458; Fax: +91 1724126261; Email: monika.sharma@plaksha.edu.in
Present address: Garima Arya, Department of Immunology and Microbiology, School of Medicine, University of Colorado—Anschutz Medical Campus, Aurora, CO 80045, USA.

Abstract

GntR/FadR family featuring an N-terminal winged helix–turn–helix DNA-binding domain and a C-terminal α-helical effector-binding and oligomerization domain constitutes one of the largest families of transcriptional regulators. Several GntR/FadR regulators govern the metabolism of sugar acids, carbon sources implicated in bacterial–host interactions. Although effectors are known for a few sugar acid regulators, the unavailability of relevant structures has left their allosteric mechanism unexplored. Here, using DgoR, a transcriptional repressor of D-galactonate metabolism in *Escherichia coli*, as a model, and its superrepressor alleles, we probed allostery in a GntR/FadR family sugar acid regulator. Genetic and biochemical studies established compromised response to D-galactonate as the reason for the superrepressor behavior of the mutants: T180I does not bind D-galactonate, and while A97V, S171L and M188I bind D-galactonate, effector binding does not induce a conformational change required for derepression, suggesting altered allostery. For mechanistic insights into allosteric communication, we performed simulations of the modeled DgoR structure in different allosteric states for both the wild-type and mutant proteins. We found that each mutant exhibits unique dynamics disrupting the intrinsic allosteric communication pathways, thereby impacting DgoR function. We finally validated the allosteric communication model by testing *in silico* predictions with experimental data.

Graphical abstract

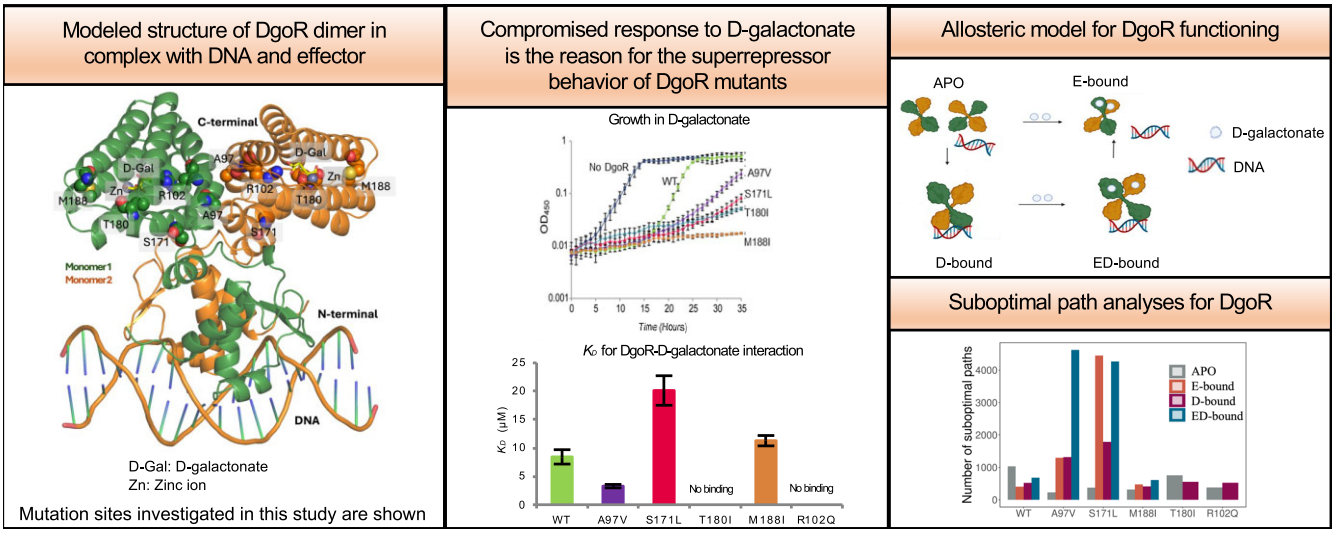

Received: December 17, 2023. **Revised:** December 14, 2024. **Editorial Decision:** December 17, 2024. **Accepted:** December 23, 2024

Introduction

Bacteria rapidly sense and adapt to changing environmental conditions by modulating gene expression, often mediated by transcriptional regulators (TRs). TRs usually sense effector molecules that alter their affinity for the operator DNA, resulting in transcriptional activation or repression of the target genes. Allostery is one of the common mechanisms that TRs use to respond rapidly to environmental cues. TRs are modular in structure, allowing them to act as regulatory switches. Here, the binding of an effector molecule at one site of the TR, i.e. the effector binding domain, changes the activity of the TR at a distant site, i.e. the DNA-binding domain (1,2). Besides a fundamental understanding of molecular processes, deeper mechanistic insights into the functioning of TRs are essential for their use in synthetic biological applications (3–10).

Bacterial TRs encompass diverse protein families, with the GntR family of TRs being among the most prevalent. These versatile regulators govern various processes such as antibiotic production, biofilm formation, development, metabolism, plasmid transfer, sporulation and virulence. GntR family members feature an N-terminal winged helix–turn–helix (wHTH) DNA-binding domain (Pfam, PF00392) and a C-terminal effector-binding and oligomerization (E-O) domain. Despite the modest sequence identity of the N-terminal domain, its overall structure remains remarkably conserved. The wHTH motif includes three α-helices, where a short turn links α-2 and α-3. The helical core is followed by two or, in some cases, three β-sheets connected by a small loop, known as the 'wing' region (2,11–13). DNA recognition patterns of GntR family TRs mainly encompass inverted repeats, although some also bind direct repeats or DNA sequences with additional symmetry (2,14–17). Several crystal structures of TRs in complex with cognate inverted repeats are available within the GntR family, such as FadR from *Escherichia coli* and *Vibrio cholerae*, NagR (previously named YvoA), and the N-terminal domain of AraR from *Bacillus subtilis* and Atu1419 from *Agrobacterium fabrum*. These structures reveal a consistent DNA-binding mode, with each TR functioning as a dimer, where each monomer recognizes half of the inverted repeat. DNA interactions involve α-2 and α-3 helices, and wing regions interacting with major and minor grooves, respectively (18–23). Atu1419 from *A. fabrum* is an exception, which binds DNA as a tetramer (21). Furthermore, cryo-electron microscopy of *E. coli* NanR complexed with its cognate DNA offers insights into GntR regulator interaction with direct repeats (14).

The diverse secondary structure and topology of the C-terminal E-O domain divide the GntR family into seven subfamilies (2,13,17,24). Aside from effector binding, the E-O domain often contributes to TR oligomerization. While not directly involved in DNA binding, the E-O domain's influence through steric constraints impacts the DNA-binding domain, affecting regulation. Notably, the FadR subfamily, which showcases an all-α-helical C-terminal E-O domain, constitutes ∼40% of GntR family members (17). FadR subfamily members primarily regulate pathways linked to carbon metabolism (13,17); their effectors typically include pathway substrates or intermediates, forming a complex regulatory network (25–34). Despite effector knowledge, conformational changes driving transcriptional regulation remain elusive in the FadR subfamily. Such understanding often relies on high-resolution TR structures in APO, DNA- and effector-bound forms for mechanistic deductions (1,2). However, within the FadR subfamily, comprehensive structures are only available for select members, including FadR from *E. coli, V. cholerae* and *Vibrio alginolyticus*, NanR from *E. coli* and Atu1419 from *A. fabrum*. These structures indicate that the binding of effector molecules in the E-O domain away from the N-terminal DNA-binding site affects transcriptional regulation. The domain rearrangement upon effector binding locks TRs in a conformation that weakens DNA binding (14,20–23,35).

Sugar acids, oxidized derivatives of sugars, have broad natural prevalence and enormous implications in bacterial–host interactions (36–49). Multiple FadR subfamily TRs regulate sugar acid metabolism. These TRs typically repress genes in the metabolic pathway, relieved upon binding of cognate effectors, which are sugar acids or pathway intermediates. The effectors have been identified for GntR from *B. subtilis* (D-gluconate), GguR from *Polaromonas* sp. strain JS666 (5-keto-4-deoxy-D-glucarate/galactarate), and DgoR (D-galactonate), ExuR (D-galacturonate and D-glucuronate) and UxuR (D-glucuronate and D-fructuronate) from *E. coli* (25,26,31–34,50,51). To date, only the crystal structure of the C-terminal E-O domain of *E. coli* DgoR is known. Efforts to elucidate the full-length structure of APO-DgoR or the E-O domain complexed with D-galactonate remain unsuccessful (52), leaving the allosteric mechanism underlying DNA release from the repressors upon effector binding largely unexplored for FadR subfamily sugar acid TRs.

We previously characterized DgoR as a FadR subfamily TR. We showed that DgoR forms dimers and represses the expression of *dgo* (D-galactonate operon) genes involved in D-galactonate metabolism by binding to two closely spaced inverted repeats in the *cis*-acting element, which overlap with the D-galactonate-inducible *dgo* promoter. We identified D-galactonate as the specific effector of DgoR. Limited proteolysis assays showed that D-galactonate binding induces a conformational change in DgoR, releasing target DNA (32,53,54) (Figure 1A). Further, using a combination of a random mutagenesis-based genetic screen to isolate DgoR superrepressors and blind docking of D-galactonate in the modeled structure of DgoR followed by in-depth genetic and biochemical analyses of the eight amino acid residues commonly identified from the two approaches, we established the D-galactonate binding cavity in the C-terminal E-O domain. Our genetic screen isolated four additional mutants in the E-O domain (A97V, S171L, T180I and M188I), which were not characterized further (53,54).

Here, through detailed genetic analyses, we validated the superrepressor behavior of A97V, S171L, T180I and M188I mutants. Biochemical analyses established that their superrepressor behavior is not because of increased affinity for the *dgo* promoter but due to compromised response to D-galactonate; T180I is unable to bind D-galactonate, and although A97V, S171L and M188I bind D-galactonate, effector binding does not induce a conformational change required for derepression, suggesting altered allostery. We further employed molecular dynamics (MD) simulations to understand the basis for the altered allosteric behavior of the mutants. We proposed a comprehensive model of allosteric communication that governs the function of DgoR. For mechanistic insights, we constructed a functional dimeric structure of DgoR and simulated it across various allosteric states (DgoR alone and DgoR bound to D-galactonate or DNA or both), for both the

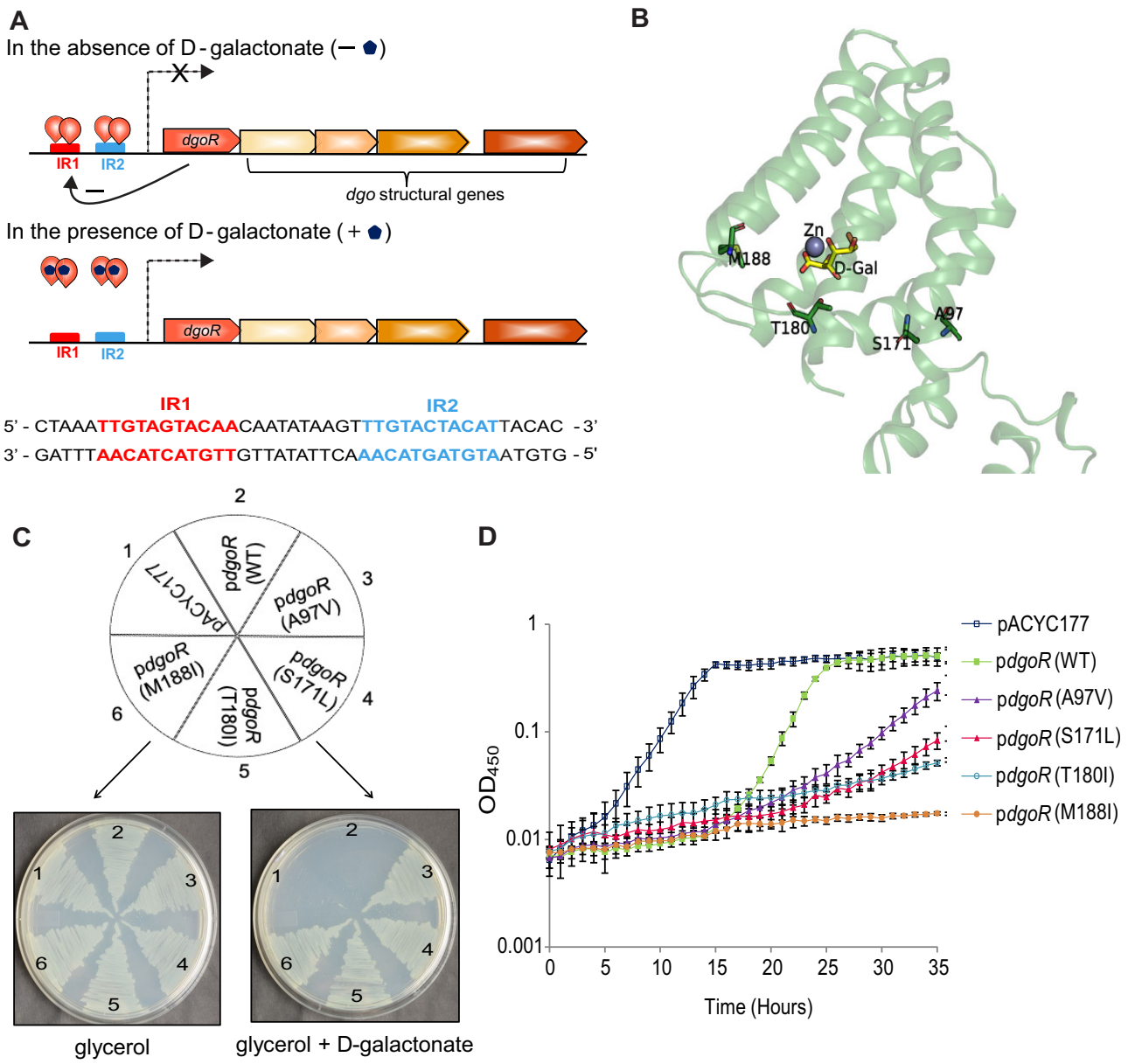

Figure 1. DgoR mutants behave as superrepressors. (**A**) Model depicting the regulation of *dgo* operon by DgoR. The transcriptional repressor, DgoR, is encoded by the first gene of the *dgo* operon, which also harbors structural *dgo* genes involved in D-galactonate transport and metabolism. Upper panel: In the absence of D-galactonate, DgoR binds two closely spaced inverted repeats (IR1 and IR2) in the *cis*-acting element that overlaps with the *dgo* promoter, thereby repressing the operon. GntR family proteins usually bind as dimers to the inverted repeat, where each monomer recognizes a half-site. Because DgoR also forms dimers, two DgoR homodimers likely bind the *dgo* promoter. Middle panel: The binding of D-galactonate induces a conformational change in DgoR, releasing the target DNA. However, whether the conformational change induced by effector binding changes the oligomeric status of the protein is unknown. Solid arrows (not drawn to scale) and bent dashed arrows denote the direction of *dgo* genes and the direction of transcription, respectively. Lower panel: The sequence of the *dgo cis*-acting element encompassing the two inverted repeats is shown. IR1 is a perfect inverted repeat, whereas IR2 has one mismatch. (**B**) Location of mutation sites in the C-terminal domain of DgoR. D-galactonate (D-Gal) in yellow sticks and Zn ion in sphere are shown. The C-terminal domain is shown in ribbon representation with residues in green sticks. (**C**) The Δ*dgoA* strain expressing DgoR mutants grows on a medium containing glycerol and D-galactonate. The Δ*dgoA* strain was individually transformed with the plasmid pACYC177, and wild-type (WT) *dgoR* or *dgoR* mutants cloned in pACYC177 [p*dgoR*(WT), pBS13; p*dgoR*(A97V), pGA33; p*dgoR*(S171L), pSW23; p*dgoR*(T180I), pGA57; and p*dgoR*(M188I), pGA58]. The transformants were streaked on M9 minimal medium containing either glycerol or glycerol and D-galactonate. The experiment was done three times. A representative image is shown. (**D**) The Δ*dgoR* strain expressing DgoR mutants either does not grow or exhibits slow growth in D-galactonate. The plasmid pACYC177 and the p*dgoR* clones mentioned in panel (C) were individually transformed in a *dgoR::kan* strain. The transformants were grown in a minimal medium supplemented with D-galactonate, and the OD_{450} was measured. The experiment was done three times, and each experiment had three technical replicates. A representative dataset, with average (±SD) from technical replicates, is shown.

WT and mutant proteins. Our findings revealed that mutations disrupt the intrinsic allosteric communication pathways, with our simulation results showing strong concordance with experimental data. Finally, we evaluated our model's predictive power through additional mutational analysis of DgoR, thereby establishing the hypothesis underlying its function.

Materials and methods

Media composition and culture conditions

The composition of the media used was as follows: lysogeny broth (LB), 5 g/l Bacto yeast extract, 10 g/l Bacto tryptone and 5 g/l NaCl; M9 minimal medium, 5.3 g/l Na_2HPO_4, 3 g/l KH_2PO_4, 0.5 g/l NaCl, 1 g/l NH_4Cl, 0.12 g/l $MgSO_4$, 2 mg/l biotin, 2 mg/l nicotinamide, 0.2 mg/l riboflavin and 2 mg/l thiamine. Where required, M9 minimal medium was supplemented with D-galactonate (10 mM, unless specified otherwise), glycerol (0.4%, vol/vol), or both glycerol and D-galactonate. Glycerol was obtained from Sigma. D-Galactonate was prepared from calcium D-galactonate (MP Biomedicals), as described (32). Difco agar (1.5%, wt/vol) was used for solidifying media. The antibiotics, ampicillin and kanamycin, were used at a concentration of 100 and 30 μg/ml, respectively, when required. Primary cultures were set up in 3 ml LB liquid medium overnight and used to inoculate secondary cultures either in LB or in M9 minimal medium containing the desired carbon source with an initial optical density (OD) of ∼0.03. The cultures were incubated at 37°C, unless mentioned otherwise.

Strains, plasmids and primers

Bacterial strains and plasmids, and primers used in this study are listed in Supplementary Tables S1 and S2, respectively. *Escherichia coli* DH5α was used for cloning in plasmids pACYC177 and pRC10. BL21(DE3) was used for expression and purification of proteins. *Escherichia coli* BW25113 and deletion strains in this background were used for various *in vivo* assays.

For fluorescence reporter assays, growth curves, analysis of superrepressor phenotype and western blotting that involved the expression of WT and mutant DgoR proteins, C-terminally 6XHis-tagged *dgoR* or its mutants cloned under the natural *dgo* promoter in pACYC177 were used. Plasmid pBS13 was used for the expression of WT DgoR (32). The *dgoR* mutants in pACYC177 were made either by subcloning the mutants obtained from the genetic screen (54) or by overlap extension polymerase chain reaction using pBS13 as the template. Plasmid pBS2 was used for overexpression and purification of C-terminally 6XHis-tagged DgoR (DgoR-6XHis) from the isopropyl-α-D-thiogalactopyranoside (IPTG)-inducible P_{trc} promoter of plasmid pRC10 (32). For the expression and purification of DgoR mutants, the mutated *dgoR* fragments amplified from their constructs in pACYC177 were cloned in pRC10.

The strains, RC12018 and RC12020, harboring single-copy transcriptional fusion of fluorescent Venus reporter with the *dgo* promoter in WT and Δ*dgoR* backgrounds, respectively, were used for fluorescence reporter assays (32).

Growth curves

Overnight cultures grown in LB were harvested, washed and resuspended in M9 minimal medium without any carbon source. Secondary cultures were set up in 200 μl M9 minimal medium supplemented with the desired carbon source to an initial OD_{450} of ∼0.03 in 96-well, clear bottom plates. Plates were incubated at 37°C in a shaker. The OD_{450} of the cultures was measured at regular intervals using a microplate reader (Tecan Infinite M200 monochromator). The shaker and microplate reader were integrated with a liquid handling system (Tecan), enabling the automated plate transfer between the two units.

Fluorescence reporter assays

Overnight cultures of reporter strains grown in LB were pelleted, washed and resuspended in an M9 minimal medium without any carbon source. Secondary cultures were grown with shaking in an M9 minimal medium supplemented with the desired carbon source, as described earlier for growth curve assays. However, here the secondary cultures were grown in 96-well, black, clear-bottom plates (Costar, Corning). Plates were incubated at 37°C with shaking. Fluorescence was measured in the exponential phase using a microplate reader (Tecan Infinite M200 monochromator) in the top mode with excitation and emission wavelengths of 498 and 568 nm, respectively (32). Fluorescence was normalized to OD_{450} and plotted in a bar or a line graph.

Western blotting

The expression of DgoR-6XHis was monitored in the exponential phase. For this, samples were electrophoresed on 15% sodium dodecyl sulfate–polyacrylamide gel electrophoresis gels and transferred to a nitrocellulose membrane. The membrane was blocked with skim milk (5%, wt/vol) at 4°C and probed with an anti-His primary antibody (1:1000; Thermo Fisher Scientific) and horseradish peroxidase-conjugated anti-mouse secondary antibody (1:5000; Sigma). Blots were developed using the SuperSignal West Dura extended-duration substrate from Pierce. The signal was detected on X-ray film or captured with an ImageQuant LAS4000 imager (GE Healthcare).

Overexpression and purification of WT and mutant DgoR-6XHis

Cultures were grown in 400 ml LB at 37°C to an OD_{600} of ∼0.8, induced with 50 μM IPTG and incubated at 18°C for 12 h. The cells were harvested, resuspended in 20 ml lysis buffer [50 mM Tris (pH 8.5), 1 M NaCl, 1 mM phenylmethylsulfonyl fluoride (PMSF) and 20 mM imidazole] and sonicated. After removing cell debris by centrifugation, the supernatant was incubated with Co-NTA beads (Pierce) on ice for 1.5 h with continuous shaking. The supernatant and beads were then transferred to a column where beads were washed successively with 30 ml wash buffer A [50 mM Tris (pH 8.5), 1 M NaCl, 10% glycerol and 20 mM imidazole] and 20 ml wash buffer B [50 mM Tris (pH 8.5), 1 M NaCl, 10% glycerol and 50 mM imidazole]. The protein was eluted in 50 mM Tris (pH 8.5), 1 M NaCl, 10% glycerol and 500 mM imidazole, and dialyzed against 50 mM Tris (pH 8.5), 1 M NaCl, 1 mM dithiothreitol (DTT) and 10% glycerol (54). The absorbance at 280 nm was measured to determine protein concentration. The concentration of WT and mutant DgoR proteins ranged from 15 to 55 μM.

Electrophoretic mobility shift assay

The 5′-end Cy5-labeled and unlabeled single-stranded complementary oligonucleotides (55 nt), corresponding to the sequence of the *dgo* promoter encompassing the DgoR binding site (from Integrated DNA Technologies), were annealed in a ratio of 1:1 to obtain labeled double-stranded DNA. Twenty microliter electrophoretic mobility shift assay (EMSA) reactions were set up, which contained 10 nM labeled double-stranded DNA, 50 mM Tris (pH 8.5), 10 mM $MgCl_2$, 265 mM NaCl, 1 mM PMSF, 12% glycerol, 2 mM DTT and 1 μg herring sperm DNA. Varying concentrations (0–1.6 μM) of purified WT DgoR or its mutants were added to the reactions. The reaction mixture was incubated at 27°C for 30 min. For experiments involving D-galactonate, DgoR was incubated with the effector at 37°C for 20 min prior to incubation with DNA. Ten microliter samples were electrophoresed on 8% native PAGE gels in 0.5× Tris–borate–EDTA buffer, pH 8.3 (45 mM Tris–borate, 1 mM EDTA) at 60 V for 2.5 h (54). Fluorescence was detected using ImageQuant LAS4000 (GE Healthcare). Both free and bound DNAs were quantified using ImageJ software (55), and the apparent K_D value for DgoR DNA interaction was calculated according to the Hill equation using Origin software version 8.5.

Microscale thermophoresis

For the K_D measurement of effector–protein interaction, serially diluted D-galactonate (100 μM to 3.05 nM) and DgoR or its mutants (500 nM) were incubated for 15 min at room temperature in a binding buffer containing 1.8 mM KH_2PO_4, 10 mM Na_2HPO_4, 137 mM NaCl, 2.7 mM KCl and 0.05% Tween 20 (pH 7.8) in a final volume of 20 μl. Subsequently, the samples were loaded into NT.LabelFree capillaries (Nano Temper Technologies). Binding experiments were conducted using a Monolith NT.LabelFree instrument (Nano Temper Technologies) with the following settings: LED power at 20% and microscale thermophoresis (MST) power set to medium. MST traces were analyzed after activating the IR laser. The results were obtained using MO Control software version 1.6, and the fraction of the formed complex was determined using MO Affinity Analysis software version 2.3. The fraction of the bound complex obtained for each concentration of D-galactonate was plotted against the effector concentration. Data were fitted to obtain the apparent K_D (56).

For the K_D measurement of DNA–protein interaction, the 5′-end Cy5-labeled double-stranded DNA template used in EMSAs was employed. Serially diluted WT DgoR or its mutants (13.75 μM to 0.42 nM) and 5′-end Cy5-labeled template (5 nM) were incubated for 15 min at room temperature in HEPES buffer (50 mM HEPES, 25 mM $MgCl_2$, 50 mM NaCl and 0.25% NP-40). After incubation, samples were loaded into Monolith NT.115-labeled capillaries (Nano Temper Technologies). Binding experiments were conducted using Monolith NT.115 with red filter (Nano Temper Technologies) with the following settings: LED power at 40% and MST power set to medium. The results were obtained using MO Control software version 1.6, and the fraction of the formed complex was determined using MO Affinity Analysis software version 2.3 (57,58). The fraction of the bound complex obtained for each protein concentration was plotted against the protein concentration. Data were fitted to obtain the apparent K_D.

Generation of structures of WT and mutants

A functional model of DgoR dimer was generated to gain molecular insights into the impact of D-galactonate binding to DgoR on the release of target DNA. Monomeric DgoR is a two-domain protein with N-terminal DNA-binding and C-terminal E-O domains. For N-terminal domain and dimeric interface modeling, the DNA-bound structure of the FadR dimer (PDB ID: 1HW2) was used as the template (23). For modeling the C-terminal domain, coordinates from the recently published X-ray structure of the monomeric C-terminal domain of DgoR (PDB ID: 7C7E) were used (52). Although the PDB ID: 7C7E provides symmetry operation (cyclic-C2, similar to 1HW2) to generate the dimeric biological assembly, it does not encompass the full-length DgoR dimer. Because the linker region and N-terminal domain interactions are critical to our study, we used FadR template for N-terminal domain and dimeric interface modeling. PDB ID: 7C7E showed Zn ion within the D-galactonate binding pocket, and thus, was retained in our modeled structure. The modeled dimeric structure was refined for various loops and minimized using Modeller v10.4 (59). Single point mutations were introduced in the WT model for A97V, S171L, T180I, M188I and R102Q using PyMOL (http://www.pymol.org/pymol). Four sets of simulations were carried out: (i) APO state—dimeric structure alone; (ii) effector-bound (E-bound) state—dimeric structure in the presence of effector; (iii) DNA-bound (D-bound) state—dimeric structure in the presence of DNA; and (iv) effector- and DNA-bound (ED-bound) state—dimeric structure in the presence of both effector and DNA. To generate E-bound and ED-bound initial coordinates, minimized structures of APO and D-bound DgoR complexes, respectively, were docked with D-galactonate using the Autodock vina module of UCSF Chimera (60). For coordinates of DNA, the bound FadR DNA sequence was mutated to the inverted repeat sequence of DgoR IR1 (5′-CTAAA**TTGTAGTACAA**CAATAT-3′/5′-ATATTG**TTGTACTACAA**TTTAG-3′) (Figure 1A) (32). The systems were minimized and simulated to allow the overall structure to achieve equilibration.

Simulation system setup

Four sets of simulations were carried out, as mentioned earlier. Each system was simulated using AMBER forcefields: ff19SB for protein (61) and OL15 for DNA (62) using GROMACS 2022 (63). The systems were solvated in a cubic box of TIP3P waters, neutralized with Na^+ and Cl^- ions, with a simulation size of ∼80 000 atoms. The solvated neutralized system was minimized, equilibrated and simulated for 400 ns. Long-range interactions were treated using the particle mesh Ewald technique (64), and a non-bonded cutoff of 12 Å was used. An integration step of 2 fs was used while all bonds were constrained using the LINCS algorithm (65,66). Using the steepest descent algorithm, the systems were minimized to eliminate any possible clashes and bad contacts. Minimization was followed by equilibration under the NVT ensemble, which was carried out in two steps. Initially, heavy atoms of the protein and DNA were restrained using position restraints of 1000 kJ/(mol nm^2) for 2 ns. During this step, minimized structures were heated gradually from 0 to 300 K at 30 K/100 ps while maintaining the restraints. Then, restraints were applied only on Cα atoms of protein and backbone atoms of DNA with a reduced force constant of 100 kJ/(mol nm^2). The structures were further equilibrated for another 1 ns using an NPT en-

semble while maintaining a simulation temperature of 300 K and a pressure of 1 atm. The restraints were removed, and the final structures were further equilibrated for 25 ns under the NPT ensemble before entering the production phase. Finally, with no restraints, production runs were carried out for 400 ns at 300 K and 1 atm. Temperature coupling was done using the velocity rescaling method with a time constant of 0.1 ps, and pressure coupling was done using an isotropic Parrinello–Rahman pressure coupling algorithm with a time constant of 2.0 and compressibility value of 4.5e−5 (67). This resulted in 20 simulations and an overall production time of 8 μs. For post-trajectory analyses of simulations, please refer to the Supplementary Data.

Results and discussion

In vivo analyses validate the superrepressor behavior of DgoR mutants

In our previous work, to identify the D-galactonate binding cavity in DgoR, we isolated *dgoR* superrepressors using a genetic screen (54). For this, we used a Δ*dgoA* strain, in which a growth inhibitory phosphorylated intermediate (2-dehydro-3-deoxy-D-galactonate 6-phosphate) accumulates due to partial metabolism of D-galactonate (68). On a minimal medium containing D-galactonate, the Δ*dgoA* strain expressing DgoR protein that binds D-galactonate and releases the *dgo* promoter fails to grow (due to the accumulation of phosphorylated intermediate) even when the medium is supplemented with another carbon and energy source, i.e. glycerol. Only the DgoR mutants non-responsive or less responsive to D-galactonate grow in the presence of D-galactonate (54). Here, we characterized the four mutants, A97V, S171L, T180I and M188I, isolated in this genetic screen, to understand the basis for their superrepressor behavior. The location of the mutation sites in the C-terminal E-O domain is shown (Figure 1B). Because the plasmid pACYC177 harboring WT *dgoR* along with its natural autoregulated *dgo* promoter [pBS13; p*dgoR*(WT)] was randomly mutagenized to create a library of mutant p*dgoR* clones for use in the genetic screen, there was a possibility that the mutant clones carried additional mutations in the plasmid backbone. Therefore, we subcloned the *dgo* promoter and *dgoR* from the mutant clones carrying the individual four amino acid changes into a clean pACYC177 backbone. We first confirmed that similar to the parental clones, these constructs also allowed the Δ*dgoA* strain to grow on a minimal medium supplemented with glycerol and D-galactonate (Figure 1C). These clones were further used in all the *in vivo* assays to validate the superrepressor behavior of the mutants.

We previously showed that compared to WT, the Δ*dgoR* strain exhibits faster growth in a minimal medium containing D-galactonate (due to constitutive expression of *dgo* genes), and this accelerated growth phenotype is complemented by WT DgoR expressed from *dgo* promoter from pACYC177 (32). Here, we compared the growth of the Δ*dgoR* strain expressing the four DgoR mutants with the strain expressing WT DgoR to assess whether the mutations compromise the response of DgoR to D-galactonate. The DgoR mutants non-responsive or less responsive to D-galactonate were expected to confer no growth or slow growth phenotype, respectively, to the Δ*dgoR* strain. The strain expressing M188I was unable to grow in D-galactonate, whereas the strain expressing A97V, S171L or T180I exhibited slower but considerable growth (Figure 1D), indicating that all four DgoR mutants are superrepressors.

We previously designed and used a chromosomal reporter construct where fluorescent Venus was placed under the control of the *dgo* promoter as a proxy for regulation of the *dgo* operon by DgoR. As expected, whereas the Δ*dgoR* strain carrying only pACYC177 showed considerable Venus expression in both non-inducing (minimal medium containing glycerol) and inducing media (minimal medium containing glycerol and D-galactonate), Δ*dgoR* expressing WT DgoR from pACYC177 exhibited considerable Venus fluorescence only in the inducing medium (Figure 2A) (32). Here, we used the Δ*dgoR* reporter strain to test whether the four DgoR mutants are induced by D-galactonate. In the inducing medium, the Δ*dgoR* strain expressing DgoR mutants non-responsive or slightly responsive to D-galactonate was expected to show Venus expression similar to or slightly higher than the reporter expression observed when the strains were grown in the non-inducing medium. We observed that the Δ*dgoR* strain expressing T180I or M188I exhibited similar Venus expression in non-inducing and inducing media, indicating that these mutants are non-responsive to D-galactonate. On the other hand, the Δ*dgoR* strain expressing A97V or S171L showed significantly higher reporter expression in the inducing medium compared to its expression in the non-inducing medium, but the reporter expression in the inducing medium was still considerably lower than that observed for Δ*dgoR* strain expressing WT DgoR, suggesting that these mutants are only slightly responsive to D-galactonate (Figure 2A). The mild inducibility of A97V and S171L explains the slow but considerable growth of the Δ*dgoR* strain expressing these mutants in D-galactonate (Figure 1D). In the above fluorescence reporter assay, we used D-galactonate at a concentration of 10 mM (Figure 2A). We thus investigated whether the inducibility of the DgoR mutants could be improved at higher D-galactonate concentrations. However, even up to 40 mM D-galactonate, there was no considerable increase in reporter expression for any of the mutants (Figure 2B). The mutants A97V and T180I allowed mild constitutive expression of the reporter in the non-inducing medium (Figure 2C), likely due to their slightly reduced affinity for the *dgo* promoter. The partial expression of the *dgo* operon due to a decreased affinity of T180I for the *dgo* promoter is also the likely reason why this mutant supports the mild growth of the Δ*dgoR* strain in D-galactonate (Figure 1D).

Being an autorepressor, the expression of WT DgoR and its various mutants from the *dgo* promoter correlates with the repression ability of the protein (32,54). To test whether this is also true for the mutants under investigation, we monitored the levels of WT DgoR and its four mutants expressed from the *dgo* promoter, from pACYC177, in a Δ*dgoR* strain in both non-inducing and inducing media. As expected, due to the relief of DgoR repression by D-galactonate, the WT protein was considerably expressed in the inducing medium compared to the non-inducing medium (Figure 2D). In the non-inducing medium, whereas S171L and M188I had expression levels similar to the WT protein, A97V and T180I showed higher expression than WT DgoR, reiterating that these two mutants likely have reduced affinity for the *dgo* promoter. In the inducing medium, the expression of T180I and M188I did not increase further, consistent with their non-inducible behavior. The expression of A97V and S171L increased in the presence of D-galactonate but to a level lower than WT

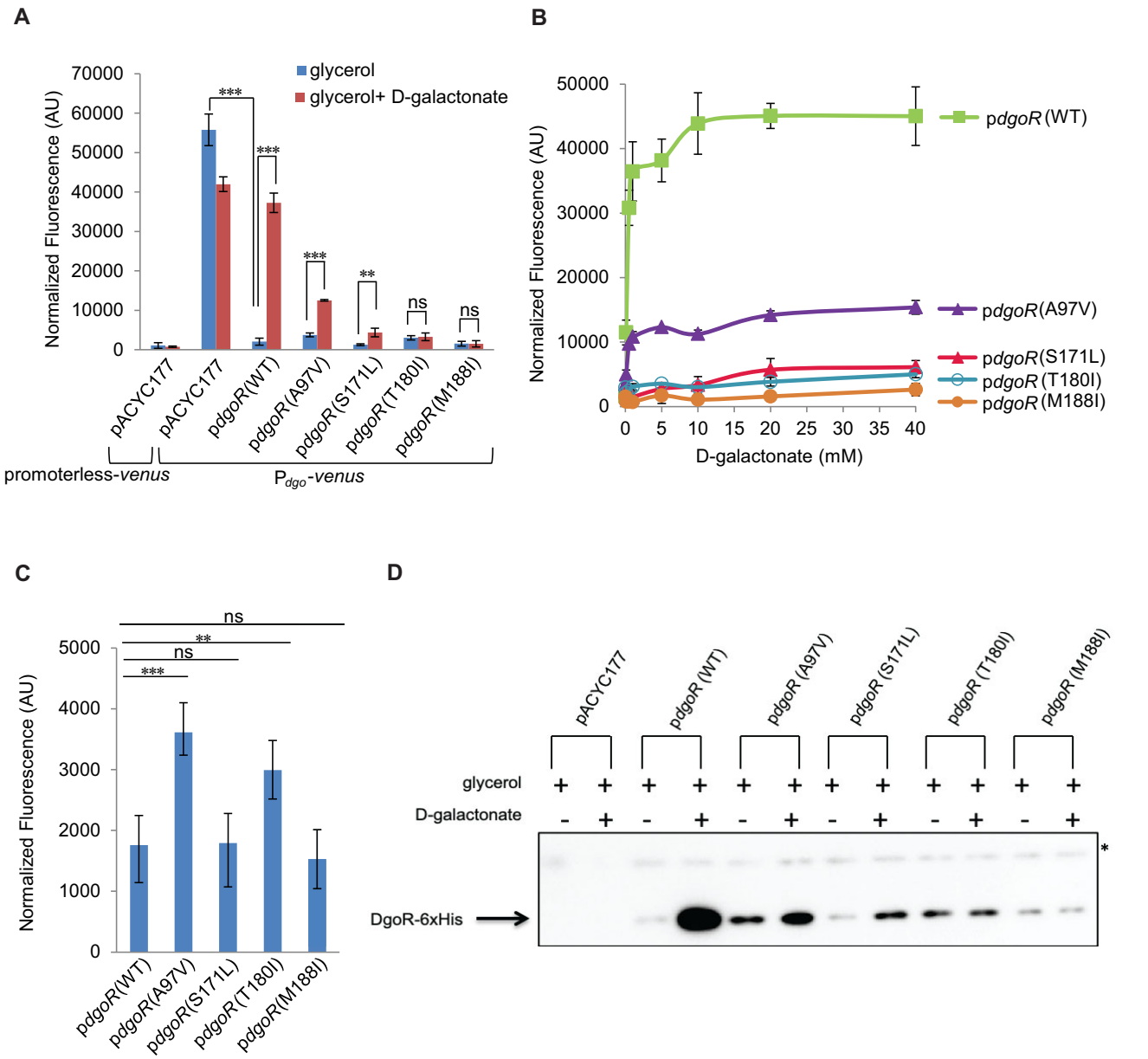

Figure 2. DgoR mutants are either not induced or slightly induced by D-galactonate. (**A**) DgoR mutants are either not induced or slightly induced by 10 mM D-galactonate. The Δ*dgoR* strain carrying the fluorescent Venus reporter on the chromosome under the control of the *dgo* promoter was transformed either with the plasmid pACYC177 or with the p*dgoR* clones mentioned in Figure 1C. The Δ*dgoR* strain carrying promoterless Venus on the chromosome and plasmid pACYC177 was used as a control for background fluorescence. Strains were grown in a minimal medium containing either glycerol or glycerol and D-galactonate. Fluorescence was measured and normalized to the OD_{450} of the samples. Data represent the average (±SD) from three independent experiments. (**B**) The inducibility of the DgoR mutants was not improved even at higher D-galactonate concentrations. The strains described in panel (A) were grown in a minimal medium supplemented either with glycerol or with glycerol and D-galactonate. The D-galactonate concentration ranged from 0.1 to 40 mM. Fluorescence was measured and normalized to the OD_{450} of the samples. Data represent the average (±SD) from at least three independent experiments. (**C**) A97V and T180I allow mild constitutive expression of the reporter in the non-inducing medium. From panels (A) and (B), the normalized fluorescence data for the Δ*dgoR* reporter strain individually transformed with the various p*dgoR* clones and cultured in a minimal medium containing glycerol were collated and plotted. Data represent the average (±SD) from at least three independent experiments. (**D**) The expression of WT DgoR and its various mutants from the natural D-galactonate-inducible promoter correlates with the repression ability of the proteins. The strains mentioned in Figure 1D were grown in a minimal medium containing either glycerol or glycerol and D-galactonate. Cells were harvested and processed for western blotting. The blot was probed with an anti-His antibody. *, Nonspecific band detected by anti-His antibody serves as a control for equal loading of samples. This blot is a representative of two independent replicates. For panels (A) and (C), the *P*-values were calculated using the unpaired two-tailed Student's *t*-test (***$P < 0.001$; **$P < 0.01$; *$P < 0.03$; ns, $P > 0.03$).

DgoR, again suggesting that these mutants are less responsive to D-galactonate than the WT protein (Figure 2D). Taken together, the expression of various DgoR proteins from the autoregulated *dgo* promoter corroborates with the expression of Venus from the *dgo* promoter in fluorescence reporter assays (Figure 2).

The superrepressor mutations are usually dominant over the WT allele (69–72). Because we used the Δ*dgoA* strain that carries a chromosomal copy of WT *dgoR* to isolate *dgoR* superrepressors (54), the four *dgoR* mutants were expected to be dominant over WT *dgoR*. Here, we further confirmed the genetic dominance of these mutants in a fluorescence reporter assay. We transformed pACYC177 carrying either WT *dgoR* or one of the four *dgoR* mutants in a WT reporter strain, i.e. WT strain carrying fluorescent Venus reporter under the control of the *dgo* promoter on the chromosome. In the presence of D-galactonate, whereas cells expressing WT DgoR either only from the chromosome or from both plasmid and chromosome exhibited considerable Venus fluorescence, cells expressing WT DgoR from the chromosome and mutant DgoR from the plasmid showed either partial (A97V) or nearly complete (S171L, T180I and M188I) repression of the Venus reporter, indicating that all four mutants are dominant over WT *dgoR* (Figure 3).

Because for all the above *in vivo* assays, WT DgoR and its mutants were expressed from the autoregulated *dgo* promoter, we confirmed that the observed phenotypes indeed reflected the repression ability of the proteins and were not due to the effect of mutations *per se* on the level of proteins. For this, we expressed WT DgoR and its mutants from a heterologous P_{trc} promoter. All four mutants expressed to a similar level as WT DgoR (Supplementary Figure S1). Collectively, the data from various *in vivo* assays establish that compared to the WT protein, the DgoR mutants, T180I and M188I, are insensitive to D-galactonate, whereas A97V and S171L are less responsive to the effector.

In vitro analyses indicate that A97V, S171L and M188I are non-/slightly responsive to D-galactonate due to altered allosteric behavior

The superrepressor phenotype of the TRs can be due to the following reasons: (i) the repressor binds the operator with increased affinity and (ii) the repressor is unable to respond to the effector, i.e. either unable to bind the effector or has altered allosteric properties such that effector binding does not induce a conformational change required for derepression (54,69,71,73,74). The amino acid residues corresponding to the four DgoR mutants lie in the C-terminal E-O domain (Figure 1B) (54). Because the C-terminal E-O domain of GntR family members is also involved in their oligomerization (2,22,75–78), which can affect the ability of the TR to bind DNA and effector, we first investigated whether the superrepressor behavior of the four DgoR mutants was due to a change in their oligomeric status. Using size exclusion chromatography, we previously showed that the DgoR protein forms dimer (54). Here, we found that the four mutants purified as C-terminally His-tagged proteins are folded and have similar retention volume on a size exclusion column as the WT protein (Supplementary Figure S2).

We next tested whether an increased affinity of DgoR mutants for the *dgo* promoter was the reason for their non-/slightly inducible behavior in the *in vivo* assays. For this, we determined the DNA binding affinity of WT DgoR and mutants in EMSAs using a fluorescently labeled double-stranded DNA probe obtained by annealing the 5′-end Cy5-labeled and unlabeled single-stranded complementary oligonucleotides of 55 nt length corresponding to the sequence of the *dgo* promoter and encompassing the two inverted repeats required for DgoR binding (54). The fluorescently labeled probe was incubated with increasing concentrations of purified WT DgoR and mutant proteins, and their apparent affinity constants (K_D) for the *dgo* promoter were determined. The apparent K_D of the three mutants that were amenable to analysis by EMSAs (A97V, S171L and T180I) ranged from 298 ± 21 to 569 ± 28 nM, comparable to the apparent K_D of WT protein (502 ± 32 nM) (Figure 4A and B). We performed MST for the M188I mutant that failed to bind the *dgo* promoter in EMSAs; WT (936 ± 97 nM) and M188I (740 ± 19 nM) bound DNA with a similar affinity (Figure 4C). Thus, for all four DgoR mutants, the increased affinity for the *dgo* promoter is not the reason for their non-/slightly inducible behavior. Although A97V and T180I mutants were mildly DNA binding defective *in vivo* (Figure 2), we could not capture their slightly altered behavior in EMSAs (Figure 4B), likely due to the differential sensitivity of the assays.

We further investigated whether the superrepressor behavior of the DgoR mutants was due to their inability to respond to the effector. For this, we first employed EMSAs to examine the ability of A97V, S171L and T180I mutants to respond to D-galactonate. Whereas D-galactonate abrogated the binding of WT DgoR to the *dgo* promoter in a concentration-dependent manner and completely released DNA fragment at 1.6 mM, D-galactonate could not significantly release *dgo* promoter bound to T180I even at ∼25 mM (Figure 5A). Further, corroborating with the mild inducible behavior of A97V and S171L *in vivo* (Figure 2), a concentration-dependent release of the *dgo* promoter was observed starting at ∼13 mM D-galactonate (Figure 5A).

Next, we performed MST to examine whether the no/mild response of the four mutants to D-galactonate is because they cannot bind or have a considerably reduced affinity for the effector. We used the R102Q mutant as a control. We previously identified R102 residue as a part of the effector binding pocket that directly interacts with D-galactonate; the R102Q mutant does not respond to D-galactonate *in vivo* and although *in vitro* it exhibits similar folding, oligomeric status and affinity for the *dgo* promoter as WT DgoR, unlike WT protein, it does not release DNA in the presence of D-galactonate (54). Here, in MST, we found that R102Q does not bind the effector, corroborating with it being a part of the effector-binding cavity. Of the four mutants investigated here, T180I did not bind the effector, while A97V had a slightly tighter affinity (K_D = 3.3 ± 0.3 μM), S171L had a slightly weaker affinity (K_D = 20.1 ± 0.6 μM) and M188I had a similar affinity (K_D = 11.3 ± 0.9 μM) for D-galactonate, when compared to the WT protein (K_D = 8.4 ± 1.3 μM) (Figure 5B and Supplementary Figure S3). Whereas the inability to bind the effector explains the non-inducible behavior of T180I, the slightly tighter affinity of A97V compared to WT protein and a comparable affinity of M188I to that of WT DgoR suggest that altered allosteric properties underlie their mild and non-responsive behavior, respectively. Similarly, the observations that S171L has only a slightly weaker affinity (∼2-fold) for the effector and that increasing D-galactonate concentration *in vivo* does not improve its inducibility (Figures 2B and 5B,

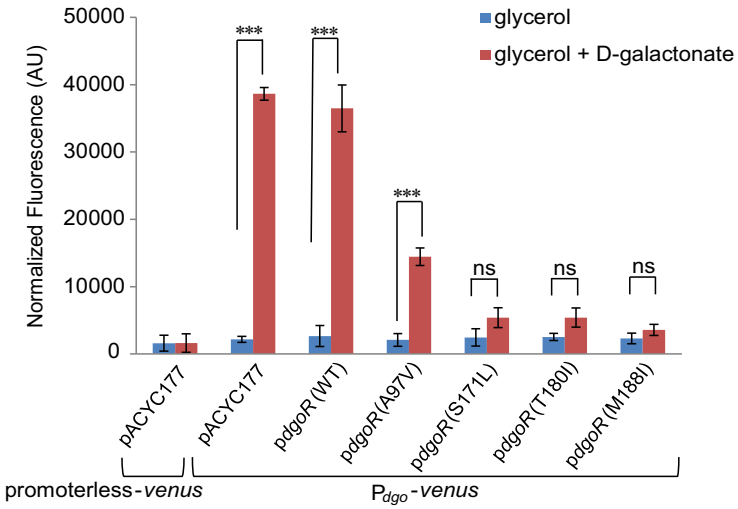

Figure 3. DgoR superrepressors are dominant over the WT. The WT strain carrying the fluorescent Venus reporter on the chromosome under the control of the *dgo* promoter was transformed either with the plasmid pACYC177 or with the p*dgoR* clones described in Figure 1C. The WT strain carrying promoterless Venus on the chromosome and plasmid pACYC177 was used as a control for background fluorescence. Strains were grown in a minimal medium supplemented either with glycerol or with glycerol and D-galactonate. Fluorescence was measured and normalized to the OD_{450} of the samples. Data represent the average (±SD) from three independent experiments. The *P*-values were calculated using the unpaired two-tailed Student's *t*-test (***$P < 0.001$; **$P < 0.01$; *$P < 0.03$; ns, $P > 0.03$).

and Supplementary Figure S3) indicates altered allostery as the major reason for its mild inducible behavior.

Using limited proteolysis, we previously showed that the binding of D-galactonate induces a conformational change in WT DgoR; the protein incubated with D-galactonate was less accessible to digestion with trypsin and showed a different digestion pattern compared to the protein incubated without the effector (32). Here, R102Q and T180I mutants that do not bind D-galactonate had a similar trypsin digestion profile in the absence or presence of effector. Among the three mutants that bind D-galactonate, a comparison of their trypsin digestion profiles in the absence and presence of effector showed that whereas A97V and S171L were less accessible to trypsin digestion and had a different digestion pattern when incubated with D-galactonate, indicating a conformational change upon effector binding, M188I had a similar trypsin digestion profile in the absence or presence of D-galactonate, suggesting that effector binding does not induce any conformational change (Figure 5B and Supplementary Figures S3 and S4). In limited proteolysis experiments, we observed that compared to the WT protein, the A97V mutant was strikingly more labile to trypsin digestion, while the M188I mutant was more resistant (Supplementary Figure S4) (discussed later).

Correlating the data from various *in vitro* assays for the binding and response of DgoR mutants to D-galactonate, the overall conclusion is as follows: (i) Because R102Q and T180I mutants are unable to bind D-galactonate, hence, even in the presence of the effector, there is no conformational change in the proteins; therefore, these mutants are non-inducible. (ii) Binding of D-galactonate to A97V and S171L induces a conformational change in the proteins; however, these mutants are unable to undergo a conformational change required for complete DNA release, resulting in a mild inducible behavior. (iii) Although D-galactonate binds M188I, effector binding does not induce any conformational change in the mutant, resulting in a non-inducible behavior.

Taken together, the detailed *in vivo* and *in vitro* analyses of the four DgoR mutants studied here show that at least A97V, S171L and M188I mutants are non-/slightly responsive to D-galactonate due to their altered allosteric behavior.

Possible mechanism of allosteric communication

We next turned to MD simulations to understand the basis of the altered allosteric behavior of the mutants. For this, drawing on our experimental data and the existing literature on similar TRs, we first considered a potential mechanism for allosteric communication that regulates the function of WT DgoR in the presence of its effector and DNA, as shown in Figure 6A. There are four predominant states available for DgoR. State A represents the APO state, where DgoR monomers form functional dimers, as suggested by experimental evidence (54) (Supplementary Figure S2B). State B represents the E-bound state, where effector molecules bind to the C-terminal domains of DgoR. State C represents the D-bound state, where DgoR binds to DNA via N-terminal domains. State D represents the ED-bound state, where the effector binds to the C-terminal domains of the DNA-bound DgoR. In this model, we assume irreversible binding of the effector and DNA, and the arrows indicate the direction of state transitions based on experimental evidence (32,54). In the APO state, DgoR can transition to the E-bound or D-bound state by binding either the effector or DNA, respectively. Upon transitioning to the E-bound state, conformational changes occur that inhibit DNA binding. Conversely, when the effector binds to the C-terminal domains of the D-bound state, DgoR undergoes conformational alterations that result in the release of DNA.

To investigate the atomistic conformational changes within DgoR complexes, we performed MD simulations of WT DgoR in four states: APO, E-bound, D-bound and ED-bound. For comparative analysis, we also modeled mutants based on experimental evidence: A97V, S171L and M188I in four states (APO, E-bound, D-bound and ED-bound)—mutants that bind both DNA and D-galactonate but are defective in releasing

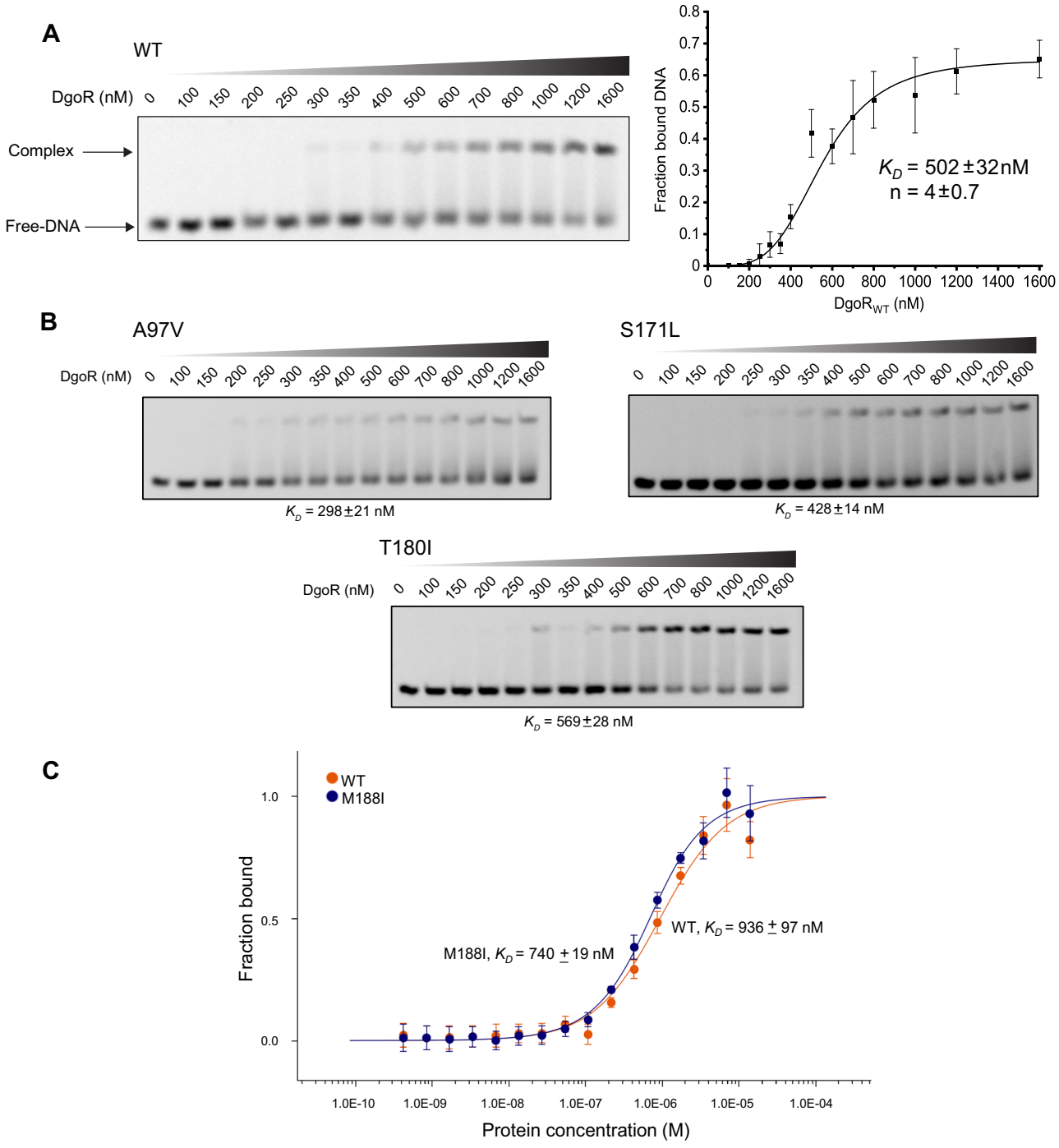

Figure 4. WT DgoR and mutants bind the *dgo* promoter with a similar affinity *in vitro*. (**A**) Determination of the apparent affinity constant (K_D) for the interaction of WT DgoR with the *dgo* promoter using EMSAs. Left: The 5′-end Cy5-labeled DNA fragment (10 nM) was incubated with indicated concentrations of WT DgoR-6XHis for 30 min, and the samples were resolved by native PAGE. Right: Bands corresponding to free DNA and protein–DNA complex were quantified to determine the apparent K_D. In the plot, each data point represents the average (±SD) of three independent assays. '*n*' is the Hill coefficient. (**B**) Determination of the apparent K_D for the interaction of DgoR mutants with the *dgo* promoter using EMSAs. The labeled probe was incubated with indicated concentrations of the DgoR mutants, and apparent K_D was measured as described in the legend to panel (A). (**C**) Determination of the apparent K_D for the interaction of WT DgoR and M188I mutant with the *dgo* promoter using MST. Serially diluted WT DgoR-6XHis and its M188I mutant (13.75 μM to 0.42 nM) and 5′-end Cy5-labeled DNA fragment (5 nM) were incubated for 15 min at room temperature and samples were loaded into labeled capillaries. Binding experiments were performed, and data were analyzed and plotted as described in the 'Materials and methods' section. In the plot, each data point represents the average (±SD) of three independent assays.

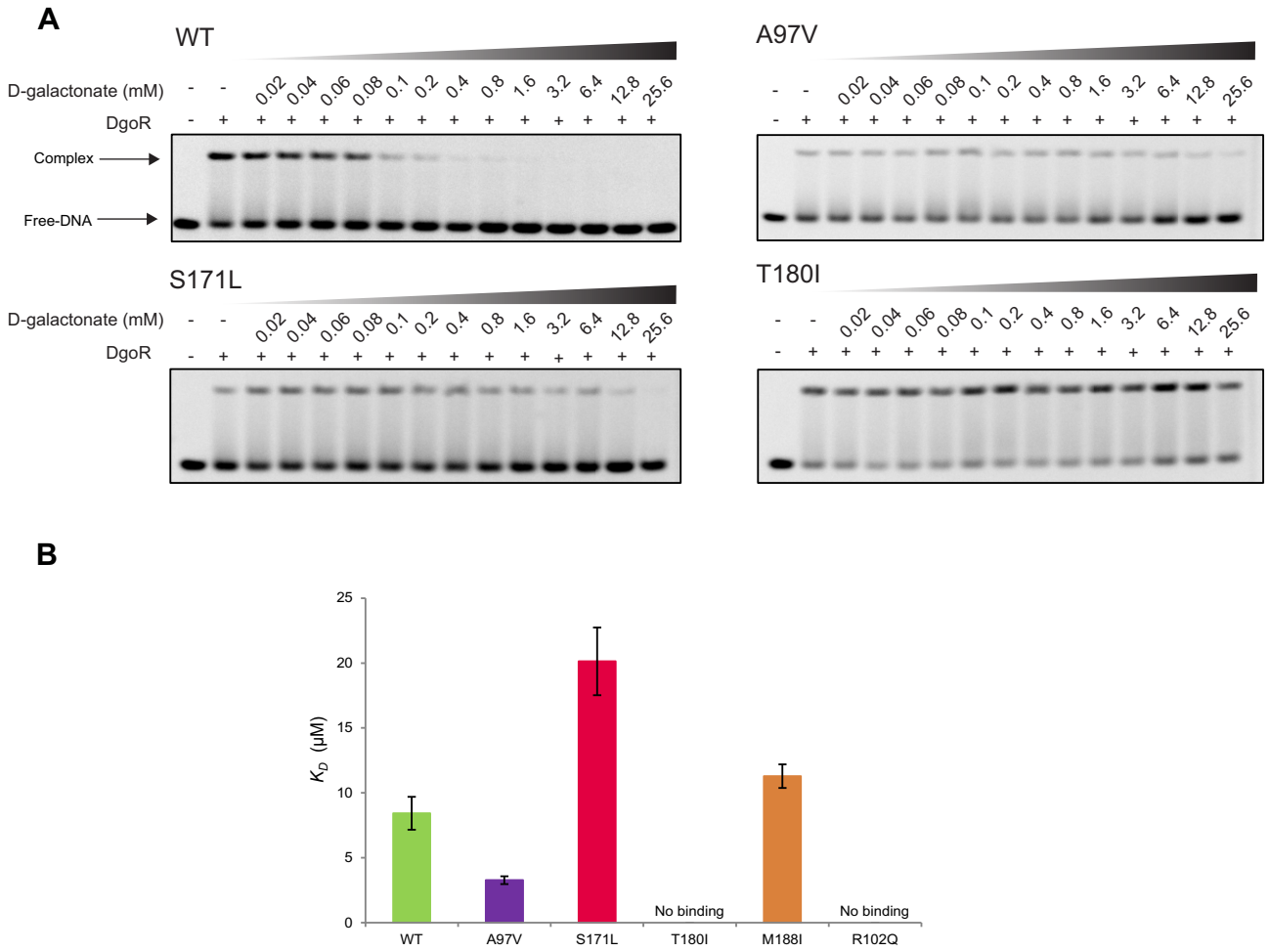

Figure 5. (**A**) DgoR mutants either do not or weakly respond to D-galactonate *in vitro*. WT DgoR-6XHis and its mutants (1 μM) were incubated with increasing concentrations of D-galactonate, as indicated, for 20 min, followed by the addition of 5′-end Cy5-labeled DNA fragment (10 nM). After incubation for 30 min, the samples were resolved by native PAGE. The experiment was performed at least two times. A representative dataset is shown. (**B**) DgoR mutants show differences in binding to D-galactonate. Serially diluted D-galactonate (100 μM to 3.05 nM) and WT DgoR-6XHis or its mutants (500 nM) were incubated at room temperature for 15 min, and the samples were loaded into label-free capillaries. Binding experiments were performed, and data were analyzed and plotted as described in the 'Materials and methods' section. The data represent the average K_D values (±SD) from three independent experiments. The representative MST plots are shown in Supplementary Figure S3.

DNA in the presence of effector; and T180I and R102Q in two states (APO and D-bound)—mutants that bind DNA but do not bind D-galactonate. We acknowledge that while the ED-bound state of WT DgoR may be a transient state, making E-bound and D-bound states the dominant states, ED-bound state remains biologically plausible and relevant. The inclusion of the ED-bound state of WT DgoR in our model enables us to investigate the structural and dynamic characteristics of this state and compare them directly to those of mutant forms.

DgoR dimeric structure bound with effector and DNA

The DgoR dimeric structure, modeled as described in the 'Materials and methods' section, served as the initial structure for all simulations (Figure 6B). DgoR is observed as a functional homodimer, with two monomers interacting side to side: the N-terminal and C-terminal domains of one monomer interact with the N-terminal and C-terminal domains of another monomer, respectively. For both the monomers, N-terminal domains interact with inverted repeats on the DNA, and C-terminal domains bind D-galactonate as an effector. The structural alignments of the Cα atoms of the modeled structure of DgoR show root mean square deviations (RMSDs) of 2.1 Å to the template (PDB ID: 1HW2) and 1.8 Å to the crystallographic symmetry-generated dimer of C-terminal domain of DgoR (PDB ID: 7C7E). Although the experimentally determined structure of DgoR provides a C-terminal domain orientation via symmetry operation, we opted for the FadR orientation, as the symmetry-generated dimer of DgoR may not accurately reflect changes due to the missing N-terminal domain and linker regions. The mutation sites simulated in this study are depicted in Figure 7. Residue A97 is involved in the dimeric interface, interacting with residues from both monomers. R102 directly interacts with the effector, as observed for D-galactonate binding pocket interactions. S171 interacts with the linker region between the N-terminal and C-terminal domains and, thus, is suggested to play a role in maintaining allosteric communication. T180 is present in the effector binding pocket and forms hydrophobic interactions

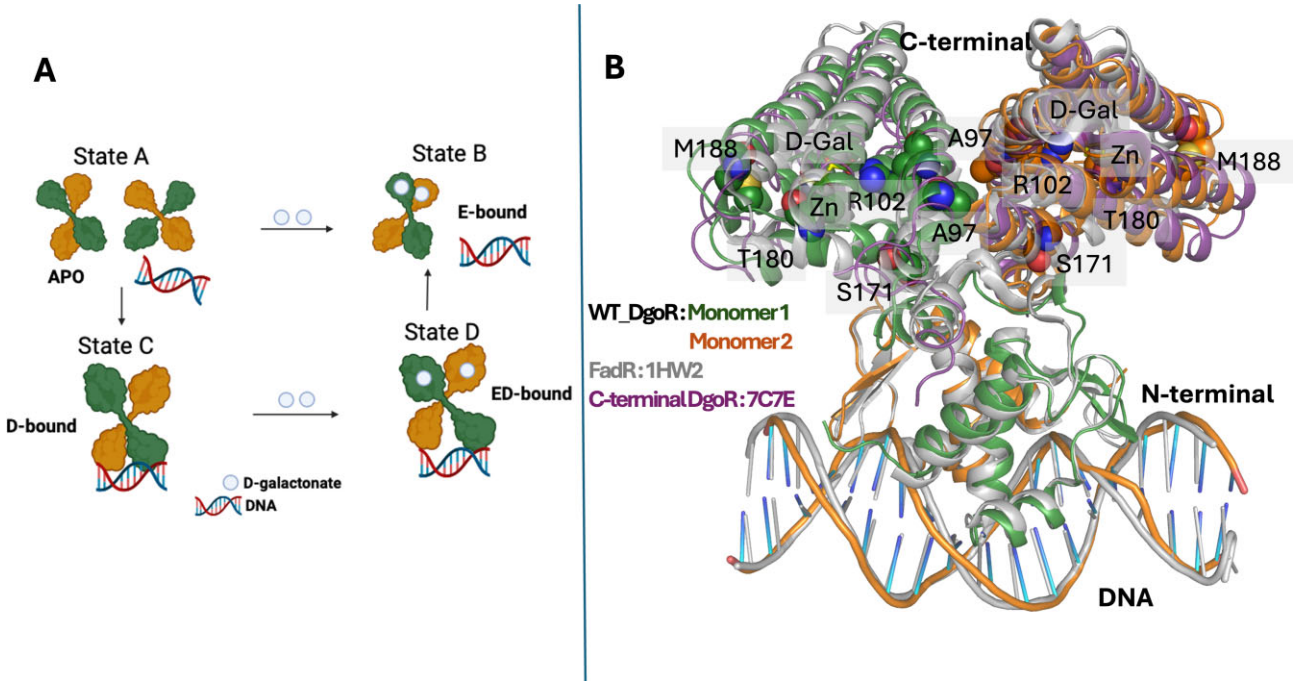

Figure 6. (**A**) Proposed allostery model of DgoR functioning. Different states and transitions are mentioned in the text. The image was created in BioRender (Chaba, R., 2024, BioRender.com/k00y485). (**B**) Modeled structure of DgoR dimer in complex with DNA and effector. The mutation sites simulated in this study are shown in spheres, and bound D-galactonate (D-Gal) is shown in sticks. Zn ion is shown in a purple sphere. Structural alignment of the model with X-ray crystal structures is shown with FadR (PDB ID: 1HW2) and the crystallographic symmetry-generated dimer of C-terminal domain of DgoR (PDB ID: 7C7E).

with the effector. M188 lines the effector binding pocket and, thus, is suggested to contribute to its stability.

Molecular simulations of WT DgoR suggest underlying allosteric communication

We analyzed the structural dynamics and allosteric communication in the dimeric full-length modeled WT DgoR across different states to understand the coupling between N-terminal DNA-binding and C-terminal E-O domains. For a detailed discussion of analyses, please refer to the Supplementary Data. Structural stability analyses using RMSD and RMSF (root mean square fluctuation) values (Figure 8A and Supplementary Figure S5) revealed significant deviations in the APO and ED-bound states, particularly in the N-terminal domain, highlighting conformational flexibility. Effector binding in the E-bound and ED-bound states induced conformational changes in the C-terminal domain, synchronizing motions across the protein and modulating DNA-binding capability. Dynamic cross-correlation (DCC) maps (Figure 8B) revealed anticorrelated motions between the N-terminal and C-terminal domains of two monomers (regions A and B) in the APO state, which diminished in the E-bound and D-bound states. In the ED-bound state, effector binding intensified anticorrelations in the N-terminal domain, resembling the APO state, suggesting an allosteric mechanism facilitating DNA release. Principal component analyses (PCAs; Figure 8C(i)) showed that effector binding in the C-terminal domain drives rotational motions in the N-terminal domain, particularly within the wHTH motif, supporting the role of long-range allosteric regulation in DNA release.

Dynamical network analyses (Figure 8C(ii)) further identified residue-level pathways underpinning allosteric communication. Community partitioning using the Girvan–Newman algorithm revealed state-specific rearrangements, with effector binding to the D-bound state (ED-bound state) increasing the number of communities, with the nucleotides of the bound DNA no longer interacting with N-terminal domain residues but instead forming their distinct communities. Suboptimal pathway analyses (Figure 8D(i)) showed reduced allosteric communication pathways in the E-bound and D-bound states compared to the APO state, while the ED-bound state exhibited an increased number of pathways, enabling alternate routes for efficient information transfer between domains. Despite state-dependent variations, the consistency in path length distributions (Figure 8D(ii)) suggests that WT DgoR maintains robust allosteric signaling across its functional states.

Mutants reveal altered conformational dynamics and allosteric communication compared to WT DgoR

Structural and dynamical analyses of DgoR mutants revealed distinct differences from WT DgoR in terms of conformational stability and allosteric regulation across functional states. For a detailed discussion of these analyses, please refer to the Supplementary Data. RMSD analyses (Figure 8A and Supplementary Figure S5) showed that while WT exhibited increased structural deviations in the ED-bound state compared to its E-bound and D-bound states, mutants showed similar or reduced deviations, indicating altered conformational dynamics.

Our limited proteolysis data suggested that A97V and M188I alter protein stability; these mutants were more and less susceptible to trypsin digestion, respectively, compared to the WT protein (Supplementary Figure S4). For comparative

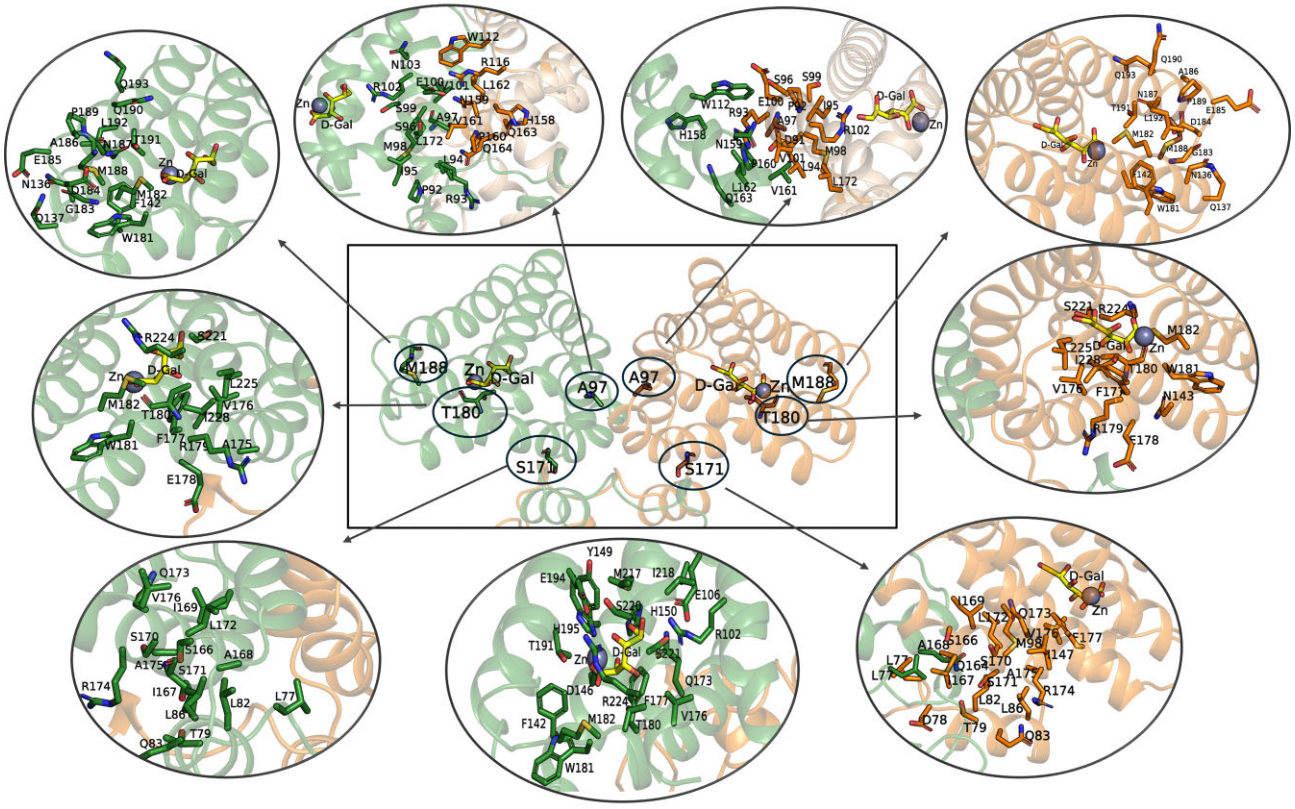

Figure 7. Detailed interactions of mutation sites simulated in this study. D-galactonate (D-Gal) in yellow sticks and Zn ion in sphere are shown. Residues in green sticks and ribbon belong to monomer 1, and residues in orange sticks and ribbon belong to monomer 2. Main chain atoms are not shown for clarity.

purposes, we measured the fraction of native contacts maintained during the simulation for APO states (Figure 8D(iii)). Looking at the relative shifts in the peak, we observed that in comparison to WT, indeed, A97V is the least stable mutant, and M188I is the most stable mutant, as indicated by the decreased and increased values of the fraction of native contacts maintained during the simulations, respectively. To further validate that these mutations alter the stability of DgoR, we determined the apparent melting temperature (T_m) of the proteins by subjecting them to thermal denaturation from 25 to 90°C and recording their circular dichroism (CD) spectra. Compared to the WT protein ($T_m = 62 \pm 0$°C), A97V had a lower T_m (56.3 ± 0.6°C), while M188I had a higher T_m (67.3 ± 0.6°C), confirming that these mutations either decreased (A97V) or increased (M188I) the stability of DgoR (Supplementary Figure S6).

DCC maps highlighted state-specific alterations in inter- and intradomain motions (Supplementary Figure S7). A97V and S171L showed increased anticorrelated motions (region A) in the E-bound state compared to WT, suggesting that effector binding in mutants is less effective at suppressing DNA-binding ability. A97V and T180I exhibited weak synchronized motions (regions C–F) in the D-bound state, indicating impaired DNA interactions. Conversely, S171L displayed strong correlations (regions C–F) in the D-bound state, suggesting favorable DNA binding, but reduced correlations in the ED-bound state, indicating more rigidity in the mutant structure that hinders DNA release. A97V exhibited intense correlations in the ED-bound state, indicating that effector binding does not favor DNA release. M188I consistently showed sparse correlations across states, reinforcing its structural rigidity and effector-insensitive behavior. R102Q showed effective synchronized motions (regions C–F) in the D-bound state, suggesting favorable DNA binding.

PCA further revealed that mutations affected essential dynamics (Supplementary Figure S8). In the APO state, mutants exhibited minimal motions, reflecting structural rigidity. In the E-bound state, while A97V and S171L showed significant interdomain fluctuations within N-terminal domains, consistent with altered correlations in DCC maps (Supplementary Figure S7), M188I showed rigid behavior. In the D-bound state, whereas T180I showed notable motions in the N-terminal domain, suggesting the impact of mutation on DNA binding, A97V, M188I and R102Q exhibited minimal motions, suggesting favorable interactions with DNA within the simulated time frame. In both the D-bound and ED-bound states, S171L showed significant motions in the N-terminal and C-terminal domains, indicating that this mutation modulates the dynamic motions of the complex, regardless of effector binding. The ED-bound states of A97V and M188I exhibited minimal motions, indicating that effector binding did not sufficiently alter DNA interactions.

Community network analyses identified changes in residue connectivity due to mutations (Supplementary Figure S9). In particular, unlike WT, substantial interactions between DNA nucleotides and N-terminal domain residues were observed in the mutants in their ED-bound states, highlighting that ef-

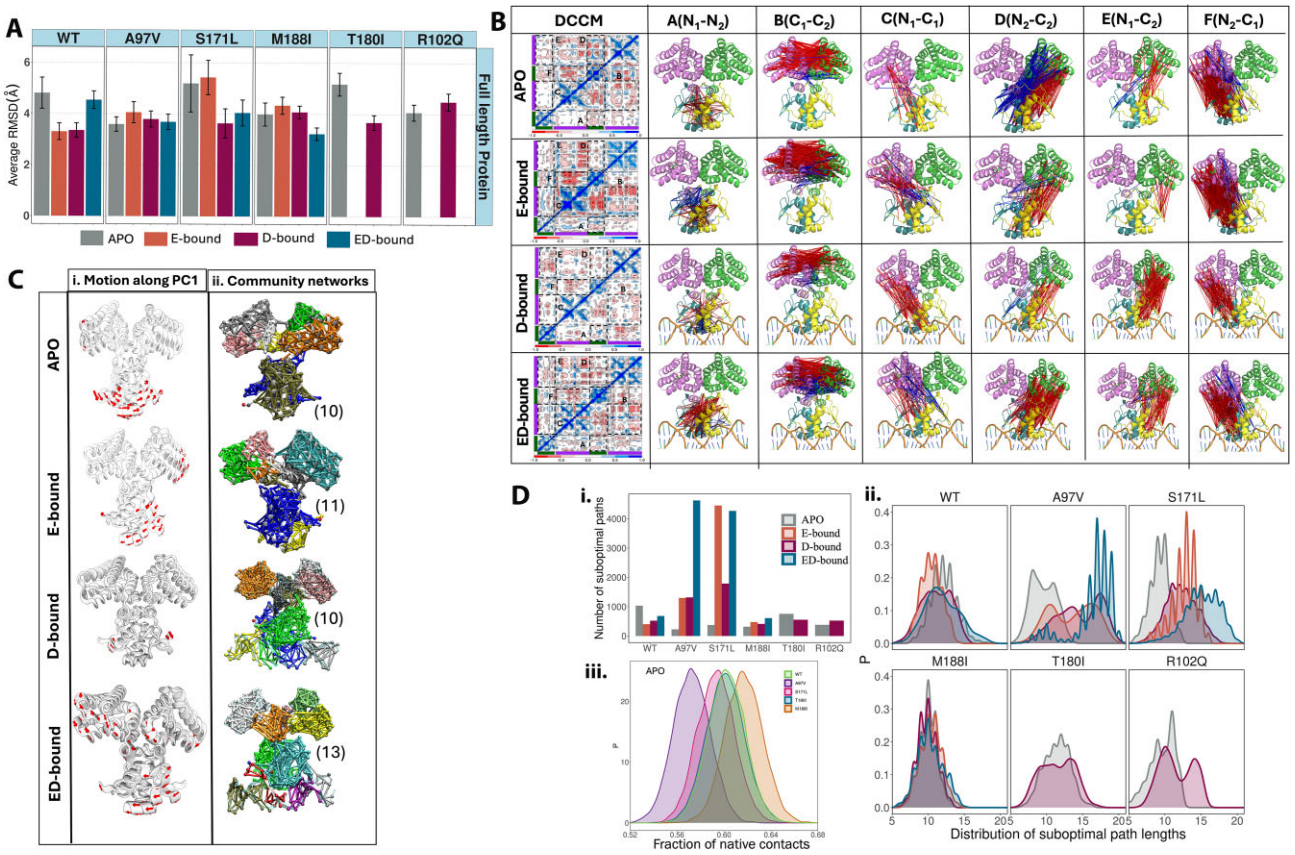

Figure 8. (**A**) Average RMSD values for backbone atoms of dimeric full-length DgoR calculated for the different states of WT and mutants. Corresponding time-evolution RMSD and RMSF plots are shown in Supplementary Figure S5. (**B**) DCC maps calculated as the time average for Cα atoms of dimeric protein for four states of WT DgoR complex. The N-terminal (residues 1–71) and C-terminal (residues 91–229) domains are annotated with boxes of green and purple, respectively. Correlation coefficients ranging from −1 to + 1 are color coded: blue for positive correlations (0.25–1), red for negative correlations (−0.25 to −1) and white for weak or no correlations (−0.25 to +0.25). For a detailed description of regions A–F and comparative DCC maps for mutant complexes, please refer to Supplementary Figure S7. The correlations within these regions are mapped to the structural regions of the WT DgoR complex with red and blue lines indicating negative and positive correlations between the residues, with subscripts 1 and 2 corresponding to monomer 1 and monomer 2, respectively. (**C**) (i) Motion along the top principal component (PC1) for four states of the WT DgoR complex. Red arrows depict the direction and magnitude of displacement with cutoff values of 3.5 Å. (ii) Networks split into distinct communities, each highlighted by a unique color, are depicted for the four states of the WT DgoR complex. The values in parentheses represent the total number of communities observed for each respective state. Motion along PC1 and community network analysis for mutants are shown in Supplementary Figures S8 and S9, respectively. (**D**) (i) Total number of suboptimal paths between the N-terminal and C-terminal regions for WT and mutant DgoR complexes across different states. (ii) Distribution of suboptimal path lengths computed for allosteric communication between the N-terminal and C-terminal domains of different states of WT and mutant DgoR complexes. (iii) Native contact analysis. Distribution of fraction of native contacts observed during simulation in APO states of WT and mutants.

fector binding did not impact the DNA release ability. Suboptimal path analyses (Figure 8D(i) and (ii)) revealed reduced allosteric communication efficiency in mutants compared to WT. In the APO state, A97V and S171L showed fewer suboptimal paths and shorter path lengths, suggesting less efficient signal transmission. Although in the E-bound, D-bound and ED-bound states, A97V and S171L showed an increased number of paths, a right-shifted path length distribution indicates inefficient communication. M188I displayed fewer paths with shorter lengths, reflecting rigidity and disrupted function. T180I and R102Q exhibited broader path length distributions, indicating compromised allosteric regulation.

Overall, these findings demonstrate that mutations disrupt the delicate balance of allosteric communication in DgoR, leading to altered conformational dynamics, impaired effector-mediated DNA release and reduced functional efficiency.

Establishing hypothesis of allosteric communication via predictive studies

Our simulation data support the proposed model of DgoR functioning, where the N-terminal and C-terminal domains allosterically modulate DgoR activity by altering its conformational dynamics in response to effector binding and DNA interaction. Effector binding in WT DgoR induces long-range allosteric communication between the C-terminal E-O and N-terminal DNA-binding domains, facilitating DNA release through dynamic conformational changes, synchronized motions and alternate communication pathways. Simulations of mutant complexes in various states revealed that these mutations affect multiple conformational states, a phenomenon challenging to discern through static structures or experiments alone. Mutating A97 at the dimeric interface to valine and S171 near the linker region to leucine (Figure 7) affects allosteric communication in all four states. In the APO state of A97V, structural destabilization indicated by the native

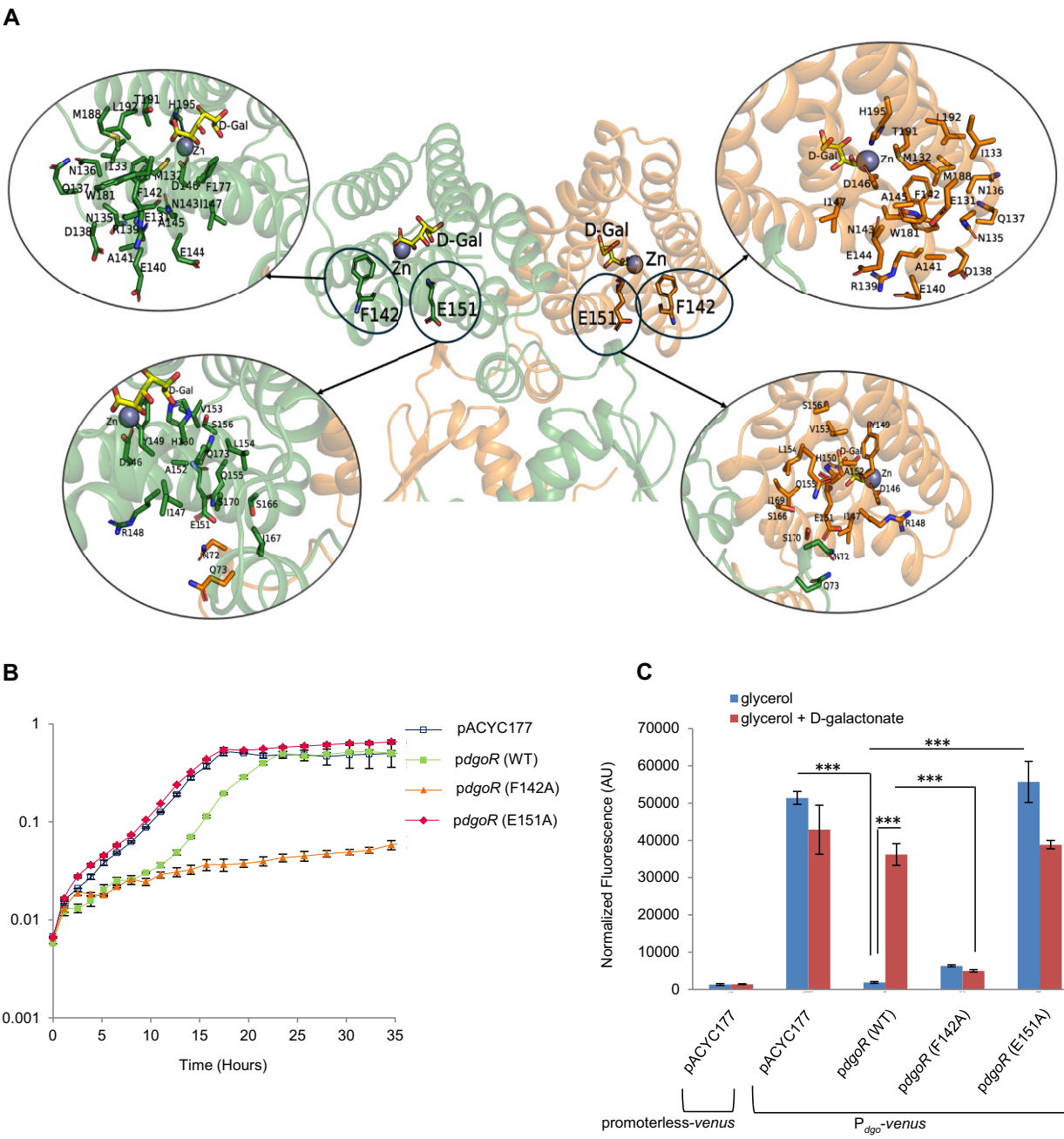

Figure 9. Predictive studies establish the hypothesis of allosteric communication. (**A**) Detailed interactions of F142 and E151 in the ED-bound state of the WT DgoR complex. D-galactonate (D-Gal) in yellow sticks and Zn ion in sphere are shown. Residues in green sticks and ribbon belong to monomer 1, and residues in orange sticks and ribbon belong to monomer 2. Main chain atoms are not shown for clarity. (**B**) F142A and E151A confer no growth and faster growth phenotype to the Δ*dgoR* strain in D-galactonate, respectively. The plasmid pACYC177 and WT *dgoR* or *dgoR* mutants cloned in pACYC177 [p*dgoR*(WT), pBS13; p*dgoR*(F142A), pGA39; and p*dgoR*(E151A), pGA44] were individually transformed in a *dgoR*::*kan* strain. The transformants were grown in a minimal medium supplemented with D-galactonate, and the OD_{450} was measured. The experiment was performed twice, and each experiment had three technical replicates. A representative dataset, with average (±SD) from technical replicates, is shown. (**C**) F142A is non-inducible, while E151A exhibits constitutive behavior. The Δ*dgoR* strain carrying the fluorescent Venus reporter on the chromosome under the control of the *dgo* promoter was transformed either with the plasmid pACYC177 or with the p*dgoR* clones mentioned in panel (B), and fluorescence reporter assays were performed as described in the legend to Figure 2A. Data represent the average (±SD) from three independent experiments. The *P*-values were calculated using the unpaired two-tailed Student's *t*-test (***$P < 0.001$).

contact analysis (Figure 8D(iii)) maps to the smaller number of suboptimal paths (Figure 8D(i)). More suboptimal path lengths for E-bound, D-bound and ED-bound states indicate that A97V and S171L mutations abolish the efficient allosteric communication (Figure 8D(ii)). Mutating M188 lining the effector binding pocket to isoleucine (Figure 7) rigidifies the structure in all four states, as indicated by average RMSD (Figure 8A), DCC maps (Supplementary Figure S7), PCA (Supplementary Figure S8), native contacts and suboptimal paths analyses (Figure 8D), preventing effective allosteric communication. T180I and R102Q affect the binding pocket of D-galactonate (Figure 7) and play a direct role in allosteric communication for DgoR functioning (Figure 8D(i) and (ii)).

By integrating network data and suboptimal path analyses obtained from simulations, we identified several residues as critical nodes for allosteric communication. Among the most frequently recurring nodes (present in over 70% of the paths), we selected two residues, F142 and E151, to validate our predictions and evaluate the reliability of our simulations. The remaining residues will be the focus of future investigations. While static structures indicated that F142 and E151 are positioned in the C-terminal domain (Figure 9A), MD simulations demonstrated the dynamic and sustained hydrogen bonding interactions between E151 and the side chain of N72 in the linker region of another monomer, as well as the functional relevance of F142 in the effector binding pocket. These findings highlighted the role of E151 in efficient allosteric communication and F142 in maintaining the integrity of the effector binding pocket, encouraging us to test their impact on DgoR function. We thus created alanine substitutions of these residues and determined the growth of mutants in D-galactonate and their inducibility in fluorescence reporter assays, as performed for the four mutants isolated in the genetic screen (Figures 1D and 2A). The Δ*dgoR* strain expressing F142A could not grow in D-galactonate, whereas the strain expressing E151A exhibited growth similar to Δ*dgoR* carrying empty plasmid (Figure 9B). Further, in contrast to the Δ*dgoR* reporter strain expressing WT DgoR, while the strain expressing F142A did not exhibit any increase in Venus expression in the inducing medium compared to its expression in the non-inducing medium, the strain expressing E151A showed a considerably high reporter expression (similar to the Δ*dgoR* carrying empty plasmid) even in the non-inducing medium (Figure 9C). Because the expression of the E151A mutant in Δ*dgoR* resulted in phenotypes similar to cells lacking DgoR, we verified its expression from the autoregulated *dgo* promoter (Supplementary Figure S10). These *in vivo* data show that F142A cannot respond to D-galactonate, consistent with being part of the effector binding pocket, while E151A is completely DNA binding defective, corroborating its role in efficient allosteric communication.

Conclusion

Using *E. coli* DgoR as a model and its superrepressor alleles, we provided the first detailed mechanistic insights into the allosteric regulation of a FadR subfamily sugar acid TR. We validated the superrepressor behavior of DgoR mutants (A97V, S171L, T180I and M188I), which were isolated in a previous genetic screen, and elucidated the molecular basis of their altered function using a combination of genetics, biochemical approaches and MD simulations. Previously, an allosteric mechanism of transcriptional regulation has been suggested through structural characterization of various members of the FadR subfamily, including *E. coli* FadR, *V. cholerae* FadR, *V. alginolyticus* FadR, *A. fabrum* Atu1419, *E. coli* NanR and *E. coli* UxuR (14,20–23,35,79). These structural studies indicated that TRs undergo dramatic conformational changes upon effector binding, enabling efficient regulation. However, conformational dynamics have only been studied for UxuR, where researchers compared the dynamics of APO UxuR to its effector-bound structures, observing significant N-terminal domain transitions within the nanosecond range. While these simulations provided insights into the conformational dynamics of TRs upon effector binding, they lacked the bound DNA structure in the N-terminal domain.

In our study, we proposed an allosteric communication model underlying the DgoR function, identifying four allosteric conformational states available for DgoR. We conducted unbiased simulations for the WT and mutant forms of DgoR to gain mechanistic insights. By combining *in silico* and experimental data, we uncovered that the mutations affect the underlying allosteric communication of different conformational states. We further validated our model by testing the predictions it generated. Our approach of identifying functionally relevant differences in communication pathways and interactions within known conformational states lays the groundwork for future efforts to directly explore transitions between states. Finally, this study offers a basis to examine the allosteric behavior of other TRs of the GntR/FadR family and improve our understanding of transcriptional regulation.

Data availability

The entire data are available in the article and in its online supplementary material.

Supplementary data

Supplementary Data are available at NAR Online.

Acknowledgements

S.S., G.A. and Sh.S. acknowledge fellowship support from IISER Mohali, the University Grants Commission (UGC) and the Council of Scientific and Industrial Research (CSIR), respectively, for doctoral work. We acknowledge the MST facility at IMTech Chandigarh and the CD facility at INST Mohali. We thank Dr Sharmistha Sinha and Ms Aarcha Radhakrishnan for their help with the thermal CD spectra experiments. We acknowledge Dr Jogender Singh, IISER Mohali, for the discussions. We thank members of the Chaba lab for discussions and critical reading of the manuscript.

Author contributions: Swati Singh: Conceptualization, Data curation, Formal analysis, Methodology (genetics and biochemical analyses), Validation, Visualization, Writing—original draft, Writing—review & editing. Garima Arya: Data curation, Formal analysis, Methodology (genetics and biochemical analyses), Validation, Writing—review & editing. Rajesh Mishra: Data curation, Formal analysis, Methodology (biochemical analyses), Validation, Visualization, Writing—review & editing. Shivam Singla: Data curation, Formal analysis, Methodology (biochemical analyses), Validation, Visualization, Writing—review & editing. Akhil Pratap: Methodology (molecular simulations), Visualization. Krishna Upadhayay: Methodology (MST), Visualization. Monika

Sharma: Conceptualization, Data curation, Formal analysis, Methodology (molecular simulations), Validation, Visualization, Writing—original draft, Writing—review & editing. Rachna Chaba: Conceptualization, Formal analysis, Methodology (genetics and biochemical analyses), Supervision, Visualization, Writing—original draft, Writing—review & editing.

Funding

This work was supported by the Department of Biotechnology (DBT) grants [BT/PR11559/BRB/10/1285/2014 to R.C. and BT/PR34553/BRB/10/1846/2020 to R.C. and M.S.] and DBT/Wellcome Trust India Alliance senior fellowship/grant [IA/S/21/2/505907 to R.C.]; and partially supported by the Department of Science and Technology-Science and Engineering Research Board (DST-SERB) grants [CRG/2018/000833 to R.C. and SB/SRS/2019-20/23/CS and SPG/2021/002604 to M.S.]; Ministry of Education-Scheme for Transformational and Advanced Research in Sciences (STARS) grant [MoE-STARS/STARS-1/296 to R.C.]; IISER Mohali and Plaksha University. Funding for open access charge: IISER Mohali.

Conflict of interest statement

None declared.

References

1. Beckett,D. (2009) Regulating transcription regulators via allostery and flexibility. *Proc. Natl Acad. Sci. U.S.A.*, **106**, 22035–22036.
2. Jain,D. (2015) Allosteric control of transcription in GntntR family of transcription regulators: a structural overview family of transcription regulators: a structural overview. *IUBMB Life*, **67**, 556–563.
3. Dietrich,J.A., Shis,D.L., Alikhani,A. and Keasling,J.D. (2013) Transcription factor-based screens and synthetic selections for microbial small-molecule biosynthesis. *ACS Synth. Biol.*, **2**, 47–58.
4. Galvão,T.C., Mencía,M. and De Lorenzo,V. (2007) Emergence of novel functions in transcriptional regulators by regression to *stem* protein types. *Mol. Microbiol.*, **65**, 907–919.
5. Jeon,Y., Lee,Y., Kim,K., Jang,G. and Yoon,Y. (2022) Transcription factor-based biosensors for detecting pathogens. *Biosensors*, **12**, 470.
6. Nasr,M.A., Timmins,L.R., Martin,V.J.J. and Kwan,D.H. (2022) A versatile transcription factor biosensor system responsive to multiple aromatic and indole inducers. *ACS Synth. Biol.*, **11**, 1692–1698.
7. Scholz,O., Köstner,M., Reich,M., Gastiger,S. and Hillen,W. (2003) Teaching TetR to recognize a new inducer. *J. Mol. Biol.*, **329**, 217–227.
8. Tang,S.-Y., Fazelinia,H. and Cirino,P.C. (2008) AraC regulatory protein mutants with altered effector specificity. *J. Am. Chem. Soc.*, **130**, 5267–5271.
9. Tang,S. and Cirino,P.C. (2011) Design and application of a mevalonate-responsive regulatory protein. *Angew. Chem. Int. Ed.*, **50**, 1084–1086.
10. Taylor,N.D., Garruss,A.S., Moretti,R., Chan,S., Arbing,M.A., Cascio,D., Rogers,J.K., Isaacs,F.J., Kosuri,S., Baker,D., *et al.* (2016) Engineering an allosteric transcription factor to respond to new ligands. *Nat. Methods*, **13**, 177–183.
11. El-Gebali,S., Mistry,J., Bateman,A., Eddy,S.R., Luciani,A., Potter,S.C., Qureshi,M., Richardson,L.J., Salazar,G.A., Smart,A., *et al.* (2019) The Pfam protein families database in 2019. *Nucleic Acids Res.*, **47**, D427–D432.
12. Hoskisson,P.A. and Rigali,S. (2009) Chapter 1: Variation in form and function. In: Laskin,A.I., Gadd,G.M. and Sariaslani,S. (eds). *Advances in Applied Microbiology*. Vol. **69**. Elsevier, pp. 1–22.
13. Rigali,S., Derouaux,A., Giannotta,F. and Dusart,J. (2002) Subdivision of the helix–turn–helix GntR family of bacterial regulators in the FadR, HutC, MocR, and YtrA subfamilies. *J. Biol. Chem.*, **277**, 12507–12515.
14. Horne,C.R., Venugopal,H., Panjikar,S., Wood,D.M., Henrickson,A., Brookes,E., North,R.A., Murphy,J.M., Friemann,R., Griffin,M.D.W., *et al.* (2021) Mechanism of NanR gene repression and allosteric induction of bacterial sialic acid metabolism. *Nat. Commun.*, **12**, 1988.
15. Quail,M.A., Dempsey,C.E. and Guest,J.R. (1994) Identification of a fatty acyl responsive regulator (FarR) in *Escherichia coli*. *FEBS Lett.*, **356**, 183–187.
16. Suvorova,I.A., Ravcheev,D.A. and Gelfand,M.S. (2012) Regulation and evolution of malonate and propionate catabolism in proteobacteria. *J. Bacteriol.*, **194**, 3234–3240.
17. Suvorova,I.A., Korostelev,Y.D. and Gelfand,M.S. (2015) GntR family of bacterial transcription factors and their DNA binding motifs: structure, positioning and co-evolution. *PLoS One*, **10**, e0132618.
18. Fillenberg,S.B., Grau,F.C., Seidel,G. and Muller,Y.A. (2015) Structural insight into operator *dre*-sites recognition and effector binding in the GntR/HutC transcription regulator NagR. *Nucleic Acids Res.*, **43**, 1283–1296.
19. Jain,D., Narayanan,N. and Nair,D.T. (2016) Plasticity in repressor–DNA interactions neutralizes loss of symmetry in bipartite operators. *J. Biol. Chem.*, **291**, 1235–1242.
20. Shi,W., Kovacikova,G., Lin,W., Taylor,R.K., Skorupski,K. and Kull,F.J. (2015) The 40-residue insertion in *Vibrio cholerae* FadR facilitates binding of an additional fatty acyl-CoA ligand. *Nat. Commun.*, **6**, 6032.
21. Vigouroux,A., Meyer,T., Naretto,A., Legrand,P., Aumont-Nicaise,M., Di Cicco,A., Renoud,S., Doré,J., Lévy,D., Vial,L., *et al.* (2021) Characterization of the first tetrameric transcription factor of the GntR superfamily with allosteric regulation from the bacterial pathogen *Agrobacterium fabrum*. *Nucleic Acids Res.*, **49**, 529–546.
22. Van Aalten,D.M.F. (2001) The structural basis of acyl coenzyme A-dependent regulation of the transcription factor FadR. *EMBO J.*, **20**, 2041–2050.
23. Xu,Y., Heath,R.J., Li,Z., Rock,C.O. and White,S.W. (2001) The FadR·DNA complex. *J. Biol. Chem.*, **276**, 17373–17379.
24. Hoskisson,P.A., Rigali,S., Fowler,K., Findlay,K.C. and Buttner,M.J. (2006) DevA, a GntR-like transcriptional regulator required for development in *Streptomyces coelicolor*. *J. Bacteriol.*, **188**, 5014–5023.
25. Bates Utz,C., Nguyen,A.B., Smalley,D.J., Anderson,A.B. and Conway,T. (2004) GntP is the *Escherichia coli* fructuronic acid transporter and belongs to the UxuR regulon. *J. Bacteriol.*, **186**, 7690–7696.
26. Bouvier,J.T., Sernova,N.V., Ghasempur,S., Rodionova,I.A., Vetting,M.W., Al-Obaidi,N.F., Almo,S.C., Gerlt,J.A. and Rodionov,D.A. (2019) Novel metabolic pathways and regulons for hexuronate utilization in proteobacteria. *J. Bacteriol.*, **201**, e00431-18.
27. DiRusso,C.C., Heimert,T.L. and Metzger,A.K. (1992) Characterization of FadR, a global transcriptional regulator of fatty acid metabolism in *Escherichia coli*. Interaction with the *fadB* promoter is prevented by long chain fatty acyl coenzyme A. *J. Biol. Chem.*, **267**, 8685–8691.
28. DiRusso,C.C., Tsvetnitsky,V., Højrup,P. and Knudsen,J. (1998) Fatty acyl-CoA binding domain of the transcription factor FadR. *J. Biol. Chem.*, **273**, 33652–33659.
29. Kalivoda,K.A., Steenbergen,S.M., Vimr,E.R. and Plumbridge,J. (2003) Regulation of sialic acid catabolism by the DNA binding protein NanR in *Escherichia coli*. *J. Bacteriol.*, **185**, 4806–4815.
30. Lee,H.Y., An,J.H. and Kim,Y.S. (2000) Identification and characterization of a novel transcriptional regulator, MatR, for

malonate metabolism in *Rhizobium leguminosarum* bv. *trifolii*. *Eur. J. Biochem.*, **267**, 7224–7230.
31. Miwa,Y. and Fujita,Y. (1988) Purification and characterization of a repressor for the *Bacillus subtilis gnt* operon. *J. Biol. Chem.*, **263**, 13252–13257.
32. Singh,B., Arya,G., Kundu,N., Sangwan,A., Nongthombam,S. and Chaba,R. (2019) Molecular and functional insights into the regulation of D-galactonate metabolism by the transcriptional regulator DgoR in -galactonate metabolism by the transcriptional regulator DgoR in *Escherichia coli*. *J. Bacteriol.*, **201**, e00281-18.
33. Tutukina,M.N., Potapova,A.V., Cole,J.A. and Ozoline,O.N. (2016) Control of hexuronate metabolism in *Escherichia coli* by the two interdependent regulators, ExuR and UxuR: derepression by heterodimer formation. *Microbiology*, **162**, 1220–1231.
34. Tutukina,M.N., Potapova,A.V., Vlasov,P.K., Purtov,Y.A. and Ozoline,O.N. (2016) Structural modeling of the ExuR and UxuR transcription factors of *E. coli*: search for the ligands affecting their regulatory properties. *J. Biomol. Struct. Dyn.*, **34**, 2296–2304.
35. Gao,R., Li,D., Lin,Y., Lin,J., Xia,X., Wang,H., Bi,L., Zhu,J., Hassan,B., Wang,S., *et al.* (2017) Structural and functional characterization of the FadR regulatory protein from *Vibrio alginolyticus*. *Front. Cell. Infect. Microbiol.*, **7**, 513.
36. BeMiller,J.N. (2008) Polysaccharides: occurrence, significance, and properties. In: Fraser-Reid,B.O., Tatsuta,K. and Thiem,J. (eds.) *Glycoscience: Chemistry and Chemical Biology*. Springer, Berlin, pp. 1413–1435.
37. Brechtel,E., Huwig,A. and Giffhorn,F. (2002) L-glucitol catabolism in -glucitol catabolism in *Stenotrophomonas maltophilia* Ac. *Appl. Environ. Microbiol.*, **68**, 582–587.
38. Ficicioglu,C., Hussa,C., Gallagher,P.R., Thomas,N. and Yager,C. (2010) Monitoring of biochemical status in children with Duarte galactosemia: utility of galactose, galactitol, galactonate, and galactose 1-phosphate. *Clin. Chem.*, **56**, 1177–1182.
39. Hommes,R.W.J., Postma,P.W., Tempest,D.W. and Neijssel,O.M. (1989) The influence of the culture pH value on the direct glucose oxidative pathway in *Klebsiella pneumoniae* NCTC 418. *Arch. Microbiol.*, **151**, 261–267.
40. Kuivanen,J., Biz,A. and Richard,P. (2019) Microbial hexuronate catabolism in biotechnology. *AMB Expr.*, **9**, 16.
41. Lai,K. and Klapa,M.I. (2004) Alternative pathways of galactose assimilation: could inverse metabolic engineering provide an alternative to galactosemic patients? *Metab. Eng.*, **6**, 239–244.
42. Peekhaus,N. and Conway,T. (1998) What's for dinner? Entner–Doudoroff metabolism in *Escherichia coli*. *J. Bacteriol.*, **180**, 3495–3502.
43. Prade,R.A., Zhan,D., Ayoubi,P. and Mort,A.J. (1999) Pectins, pectinases and plant–microbe interactions. *Biotechnol. Genet. Eng.*, **16**, 361–392.
44. Conway,T. and Cohen,P.S. (2015) Commensal and pathogenic *Escherichia coli* metabolism in the gut. *Microbiol. Spectr.*, **3**, 3.3.24.
45. Faber,F., Tran,L., Byndloss,M.X., Lopez,C.A., Velazquez,E.M., Kerrinnes,T., Nuccio,S.-P., Wangdi,T., Fiehn,O., Tsolis,R.M., *et al.* (2016) Host-mediated sugar oxidation promotes post-antibiotic pathogen expansion. *Nature*, **534**, 697–699.
46. Jimenez,A.G., Ellermann,M., Abbott,W. and Sperandio,V. (2019) Diet-derived galacturonic acid regulates virulence and intestinal colonization in enterohaemorrhagic *Escherichia coli* and *Citrobacter rodentium*. *Nat. Microbiol.*, **5**, 368–378.
47. Sweeney,N.J., Laux,D.C. and Cohen,P.S. (1996) *Escherichia coli* F-18 and *E. coli* K-12 *eda* mutants do not colonize the streptomycin-treated mouse large intestine. *Infect. Immun.*, **64**, 3504–3511.
48. Mole,B., Habibi,S., Dangl,J.L. and Grant,S.R. (2010) Gluconate metabolism is required for virulence of the soft-rot pathogen *Pectobacterium carotovorum*. *Mol. Plant Microbe Interact.*, **23**, 1335–1344.
49. Rosay,T., Jimenez,A.G. and Sperandio,V. (2024) Glucuronic acid confers colonization advantage to enteric pathogens. *Proc. Natl Acad. Sci. U.S.A.*, **121**, e2400226121.
50. Fujita,Y. and Miwa,Y. (1989) Identification of an operator sequence for the *Bacillus subtilis gnt* operon. *J. Biol. Chem.*, **264**, 4201–4206.
51. Yoshida,K., Fujita,Y. and Sarai,A. (1993) Missense mutations in the *Bacillus subtilis gnt* repressor that diminish operator binding ability. *J. Mol. Biol.*, **231**, 167–174.
52. Lin,Z., Sun,Y., Liu,Y., Tong,S., Shang,Z., Cai,Y. and Lin,W. (2020) Structural and functional analyses of the transcription repressor DgoR from *Escherichia coli* reveal a divalent metal-containing D-galactonate binding pocket. *Front. Microbiol.*, **11**, 590330.
53. Singh,S., Gola,C., Singh,B., Agrawal,V. and Chaba,R. (2024) D-galactonate metabolism in enteric bacteria: a molecular and physiological perspective. *Curr. Opin. Microbiol.*, **81**, 102524.
54. Arya,G., Pal,M., Sharma,M., Singh,B., Singh,S., Agrawal,V. and Chaba,R. (2021) Molecular insights into effector binding by DgoR, a GntR/FadR family transcriptional repressor of D-galactonate metabolism in *Escherichia coli*. *Mol. Microbiol.*, **115**, 591–609.
55. Schneider,C.A., Rasband,W.S. and Eliceiri,K.W. (2012) NIH Image to ImageJ: 25 years of image analysis. *Nat. Methods.*, **9**, 671–675.
56. Seidel,S.A.I., Wienken,C.J., Geissler,S., Jerabek-Willemsen,M., Duhr,S., Reiter,A., Trauner,D., Braun,D. and Baaske,P. (2012) Label-free microscale thermophoresis discriminates sites and affinity of protein–ligand binding. *Angew. Chem. Int. Ed.*, **51**, 10656–10659.
57. Swain,M., Ageeli,A.A., Kasprzak,W.K., Li,M., Miller,J.T., Sztuba-Solinska,J., Schneekloth,J.S., Koirala,D., Piccirili,J., Fraboni,A.J., *et al.* (2021) Dynamic bulge nucleotides in the KSHV PAN ENE triple helix provide a unique binding platform for small molecule ligands. *Nucleic Acids Res.*, **49**, 13179–13193.
58. Gao,Y., Cao,D., Pawnikar,S., John,K.P., Ahn,H.M., Hill,S., Ha,J.M., Parikh,P., Ogilvie,C., Swain,A., *et al.* (2020) Structure of the human respiratory syncytial virus M2-1 protein in complex with a short positive-sense gene-end RNA. *Structure*, **28**, 979–990.
59. Webb,B. and Sali,A. (2016) Comparative protein structure modeling using MODELLER. *Curr. Protoc. Bioinformatics*, **54**, 5.6.1–5.6.37.
60. Pettersen,E.F., Goddard,T.D., Huang,C.C., Couch,G.S., Greenblatt,D.M., Meng,E.C. and Ferrin,T.E. (2004) UCSF Chimera—a visualization system for exploratory research and analysis. *J. Comput. Chem.*, **25**, 1605–1612.
61. Tian,C., Kasavajhala,K., Belfon,K.A.A., Raguette,L., Huang,H., Migues,A.N., Bickel,J., Wang,Y., Pincay,J., Wu,Q., *et al.* (2020) ff19SB: amino-acid-specific protein backbone parameters trained against quantum mechanics energy surfaces in solution. *J. Chem. Theory Comput.*, **16**, 528–552.
62. Galindo-Murillo,R., Robertson,J.C., Zgarbová,M., Šponer,J., Otyepka,M., Jurečka,P. and Cheatham,T.E. (2016) Assessing the current state of amber force field modifications for DNA. *J. Chem. Theory Comput.*, **12**, 4114–4127.
63. Abraham,M.J., Murtola,T., Schulz,R., Páll,S., Smith,J.C., Hess,B. and Lindahl,E. (2015) GROMACS: high performance molecular simulations through multi-level parallelism from laptops to supercomputers. *SoftwareX*, **1–2**, 19–25.
64. Darden,T., York,D. and Pedersen,L. (1993) Particle mesh Ewald: an $N \cdot \log(N)$ method for Ewald sums in large systems. *J. Chem. Phys.*, **98**, 10089–10092.
65. Hess,B., Bekker,H., Berendsen,H.J.C. and Fraaije,J.G.E.M. (1997) LINCS: a linear constraint solver for molecular simulations. *J. Comput. Chem.*, **18**, 1463–1472.
66. Hess,B. (2008) P-LINCS: a parallel linear constraint solver for molecular simulation. *J. Chem. Theory Comput.*, **4**, 116–122.
67. Bussi,G., Donadio,D. and Parrinello,M. (2007) Canonical sampling through velocity rescaling. *J. Chem. Phys.*, **126**, 014101.

68. Cooper,R.A. (1978) The utilisation of D-galactonate and D-2-oxo-3-deoxygalactonate by *Escherichia coli* K-12. Biochemical and genetical studies. *Arch. Microbiol.*, **118**, 199–206.
69. Chakravartty,V. and Cronan,J.E. (2012) Altered regulation of *Escherichia coli* biotin biosynthesis in BirA superrepressor mutant strains. *J. Bacteriol.*, **194**, 1113–1126.
70. Muro-Pastor,A.M. and Maloy,S. (1995) Proline dehydrogenase activity of the transcriptional repressor PutA is required for induction of the *put* operon by proline. *J. Biol. Chem.*, **270**, 9819–9827.
71. Tian,G. and Maas,W.K. (1994) Mutational analysis of the arginine repressor of *Escherichia coli*. *Mol. Microbiol.*, **13**, 599–608.
72. Zhou,Y.N., Chatterjee,S., Roy,S. and Adhya,S. (1995) The non-inducible nature of super-repressors of the *gal* operon in *Escherichia coli*. *J. Mol. Biol.*, **253**, 414–425.
73. Alekshun,M.N. and Levy,S.B. (1999) Characterization of MarR superrepressor mutants. *J. Bacteriol.*, **181**, 3303–3306.
74. Klig,L.S. and Yanofsky,C. (1988) Increased binding of operator DNA by *trp* superrepressor EK49. *J. Biol. Chem.*, **263**, 243–246.
75. Gao,Y.-G., Yao,M., Itou,H., Zhou,Y. and Tanaka,I. (2007) The structures of transcription factor CGL2947 from *Corynebacterium glutamicum* in two crystal forms: a novel homodimer assembling and the implication for effector-binding mode. *Protein Sci.*, **16**, 1878–1886.
76. Lord,D.M., Uzgoren Baran,A., Soo,V.W.C., Wood,T.K., Peti,W. and Page,R. (2014) McbR/YncC: implications for the mechanism of ligand and DNA binding by a bacterial GntR transcriptional regulator involved in biofilm formation. *Biochemistry*, **53**, 7223–7231.
77. Resch,M., Schiltz,E., Titgemeyer,F. and Muller,Y.A. (2010) Insight into the induction mechanism of the GntR/HutC bacterial transcription regulator YvoA. *Nucleic Acids Res.*, **38**, 2485–2497.
78. Rezácová,P., Krejciríková,V., Borek,D., Moy,S.F., Joachimiak,A. and Otwinowski,Z. (2007) The crystal structure of the effector-binding domain of the trehalose repressor TreR from *Bacillus subtilis* 168 reveals a unique quarternary assembly. *Proteins*, **69**, 679–682.
79. Almeida,B.C., Kaczmarek,J.A., Figueiredo,P.R., Prather,K.L.J. and Carvalho,A.T.P. (2021) Transcription factor allosteric regulation through substrate coordination to zinc. *NAR Genom. Bioinform.*, **3**, lqab033.

Received: December 17, 2023. **Revised:** December 14, 2024. **Editorial Decision:** December 17, 2024. **Accepted:** December 23, 2024